MAE 108 Design Experiment:
Biplane Wing and Stagger (R.A.F 15)

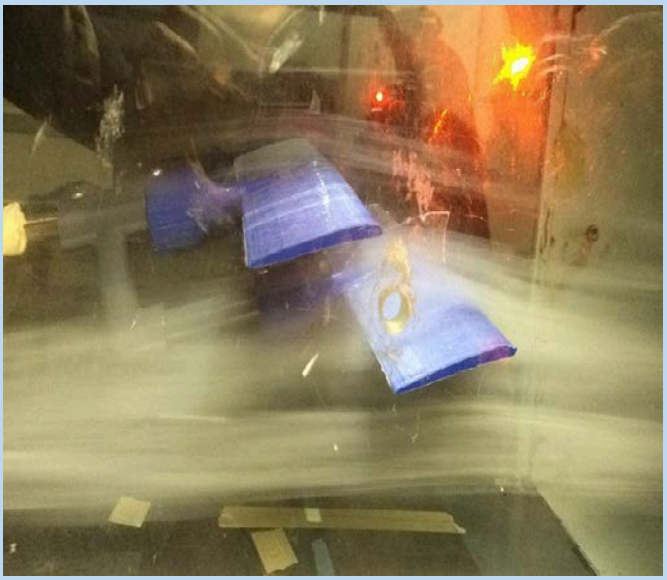

To: Manuel Gamero Castano

From: Kushal Shah

Mechanical and Aerospace Engineering

Date: 9 December 2013

UCIRVINE | THE HENRY SAMUELI SCHOOL OF ENGINEERING

Table of Contents

List of Figures

List of Tables

Nomenclature

Chord length – c

Span Length – S

Area – A

Free stream Density of air - ρ_∞

Free stream Velocity - V_∞

Free stream Dynamic Pressure - q_∞

Angle of Attack – α

Normal Force – F_N

Axial Force – F_a

Lift – $L\ or\ F_L$

Drag - $D\ or\ F_D$

Lift Coefficient - C_L

Drag Coefficient - C_D

Induced Drag Coefficient - C_{D_I}

2D Lift Slope - a

3D Lift Slope - a_o

Wing Efficiency – e

Aspect Ratio - AR

Pressure - p

Specific gas constant for dry air– R

Temperature – T

Relative Humidity - $\emptyset$

1. Abstract

The Wright Flyer was the first aircraft to fly. It used biplane design. Biplane wing has a structural advantage over a monoplane, but it produces more drag and more lift compare to similar monoplane wing. Due to its advantage of structure, they were widely used in the early years of aviation. This was the motivation for the experiment. The experiment was conducted to analyze and compare the aerodynamic performance for bi plane airfoil in single wing, biplane wing and stagger configurations. In these different configurations, the lift and drag were measured and then they were compared to similar experimental trends presented in the N.A.C.A's report no. 70 [3]. It was found that the biplane wing configuration produced higher lift and drag compared to single wing configuration. However, both wings combined are not able to produce twice as much lift as a single wing of similar size and shape because the upper and the lower are working on nearly the same portion of the atmosphere; as a result, they interfere with each other's behavior. Furthermore, it was also concluded that the positive stagger configuration provided better aerodynamic performance compared to negative stagger configuration because the lift was increased and the drag was increased slightly. However, there were discrepancies observed for the Lift Drag ratio for the biplane configurations due to increased drag on the wing that resulted from wing's mounting structure. It was also observed that the method of recording the angle of attack was not ideal and may contributed to large discrepancies in the experiment data. In conclusion, it was observed that the biplane configuration provided more lift and drag compared to single wing configuration, and the positive staggered configuration provided similar trends of increased lift and increased drag when compared to negative staggered configuration.

2. Overview

(a) Purpose and Objective

The primary purpose of this experiment is to understand and gain familiarity of the characteristics of R.A.F 15 airfoils and understand stagger configuration of the airfoil. The objective of the lab was defined as to measure the Lift, Drag, and Lift-Drag ratio of a R.A.F airfoil in single wing, bi plane wings, and various stagger configurations while varying the angle of attack.

(b) Introduction

The Wright Flyer was the first aircraft to fly. It used biplane design. Most aircraft in the early years of aviation used similar design. Biplane wind has a structural advantage over a monoplane, but it produces more drag and more lift compare to similar monoplane wing. Due to its advantage of structure, they were widely used in the early years of aviation. The biplane aircraft has two main wings, one wing is on upper surface and the second one is on lower surface. Both provide part of the lift, although they are not able to produce twice as much lift as a single wing of similar size and shape because the upper and the lower are

working on nearly the same portion of the atmosphere. As a result they interfere with each other's behavior. Biplane can lift up to 20 percent more than can a similarly sized monoplane of similar wingspan [1]. There are different configurations that are sometime used. Staggered configuration is one of the configuration and it has one wing move forward or backward respect to each other. This configuration has some advantages from the point of visibility. Two of those configuration is positive staggered configuration and negative staggered configuration. In the positive staggered configuration, the upper wing is moved forward compared to lower wing and in the negative configuration, the lower wing is moved forward compared to upper wing. Two aircrafts that used RAF-15 for its section were Thomas-Morse MB3 and Vickers Vimy (figure 3.4).

(c) Outline / Scope

This report explains the method of the experiment and the analysis of the results obtained from the experiment which allows to understand the performance of R.A.F 15 in in single wing, bi plane wings, and various stagger configurations while varying the angle of attack. First part of the report gives the introduction and background of the airfoil and its usage in the past. Then the report gives the methods used and instruments used to perform the experiment. Next, the report illustrates the results of these different configurations, where different curves are plotted to compare the trends with N.A.C.A results and Airfoil Tools results. Then, report provides discussion on the analysis of the data and the summary of key results obtained from the experiment. Finally, the report provides the sources of error attached, conclusion and recommendations for further study of the subject.

3. Historical Background

By 1896 Octave Chanute was flying a biplane hang glider and concluded that the externally-braced biplane offered better prospects for powered flight than the monoplane. The Wright flyer biplane of 1903 was the first successful airplanes. The weakness of the materials and design techniques available made it difficult to design wings which were both light and strong enough to fly. By the First World War biplanes had started to gain favor due to their maneuverability and strength. During the period from 1914 to 1925 almost all aircraft were biplanes.

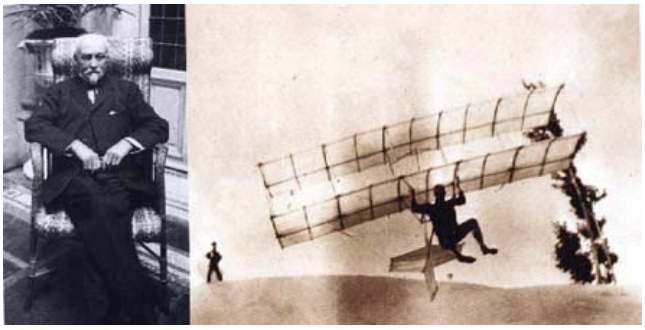

Figure 3.1: Octave's Biplane Hang Glider

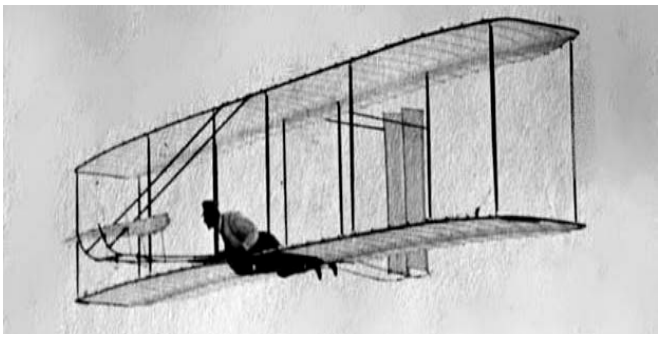

Figure 3. 2: The Wright Flyer Biplane

Figure 3. 3: The Waco *YKS-6*

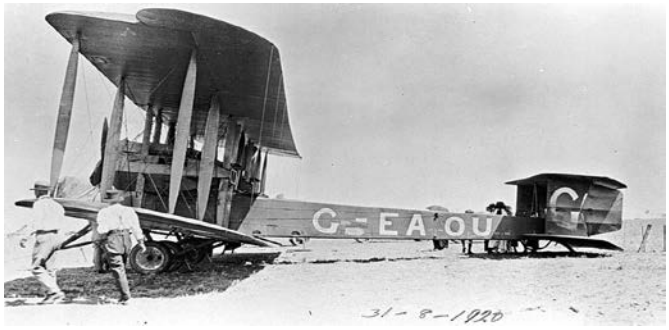

Figure 3. 4: Vickers Vimy

A common example for staggered biplane from the 1930s is the layout of Waco Standard Cabin series (figure 3.3). It is also possible to place the lower wing's leading edge ahead of the upper wing, giving negative stagger. Examples of negative stagger include the Airco DH.5, Sopwith Dolphin and Beechcraft Staggerwing. However forward stagger is more common because it improves both downward visibility. This configuration also provides ease of cockpit access for open cockpit biplanes. The widespread use of biplanes lasted from the Wright brothers' first flight in 1903 until the 1940's, when monoplanes dominated the skies in World War II. Improved structural techniques, better materials and the mission for greater speed made the biplane configuration obsolete by the late 1930s.

4. Theoretical Background and Previous Work

N.A.C.A report no. 71 thought that before they can consider the value and advantages that are related to biplane, a detailed and complete investigation of the aerodynamic effects of the stagger and biplane would be beneficial. This was the previous work that was done on the stagger of the biplanes using the R.A.F 15 and U.S.A 15 wings [3].

Using the newton's third law, the fluid and wing applies same but opposite amount of force, and Navier stroke equations, the normal and axial components that wing experiences can be determined. Then using second axis rotation and change of frame, the lift and drag can be computed. (This is also shown in the Appendix A.2).

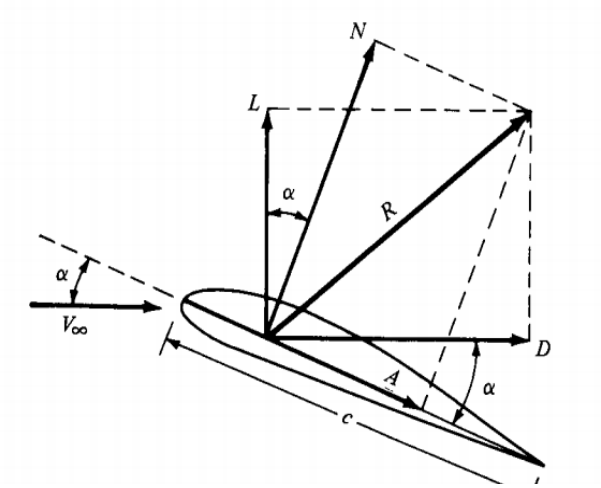

Figure 4.1: Conventions of Frame Used

$$F_L = F_N \cos(\alpha) - F_a \sin(\alpha) \text{ ……..} \text{ [Eqn 1.5]}$$

$$F_D = F_a \cos(\alpha) + F_N \sin(\alpha) \text{……} \text{ [Eqn 1.6]}$$

$Where,\ F_L$ = Lift Force, F_D = Drag Force, F_N = Normal Force, F_a = Axial Force, $\alpha - angle\ of\ attack$

$$C_L = \frac{F_L}{q_\infty * c * s} \text{ ……} \text{ [Eqn 1.9]}$$

$$C_D = \frac{F_D}{q_\infty * c * s} \text{ ……} \text{ [Eqn 1.10]}$$

5. Experimental Apparatus and Procedure

(a) Airfoil Properties and Methodology used for this experiment

The wings used in the experiment had section profile of R.A.F. 15. The R.A.F 15 airfoil has max thickness 6.5% at 15% chord and max camber 2.6% at 30% chord. Its chord length is 5.84 cm and 24 cm [5].

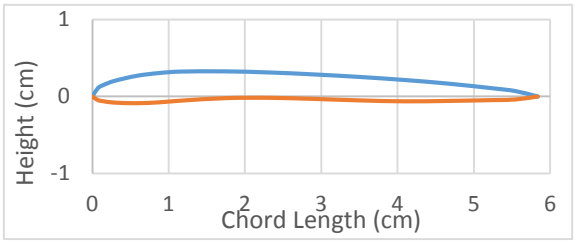

Figure 5. 1: Airfoil Tools Profile

Figure 5. 2: 3D Printed Airfoil

They were held together by PVC pipe that mounted on the sting balance Nano 17 (see figure 5.5). There were multiple PVC pipe cutouts according to needed values for stagger. These were replaced every run to get the desired stagger. The targeted speed used for the airfoil was 15 m/s and the Re # was approximately 50,000.

(b) Instruments Used

In The equipment used for the experiment consisted of the 3D printer, PVC pipes, the wind tunnel, the force balance (Nano 17), various weights, a digital analog converter (DAC), and LabView. Using the 3D Printer and the airfoil tools data, the wings were printed. Then, using the PVC pipes flexible testing apparatuses were created (figure 5.5). The wind tunnel with a “closed” test section used in the lab to set up the desired speed. For the calibration purposes and measuring Lift and Drag, the weights, DAC, LabView and the force balance were used.

(c) Block Diagram of the System

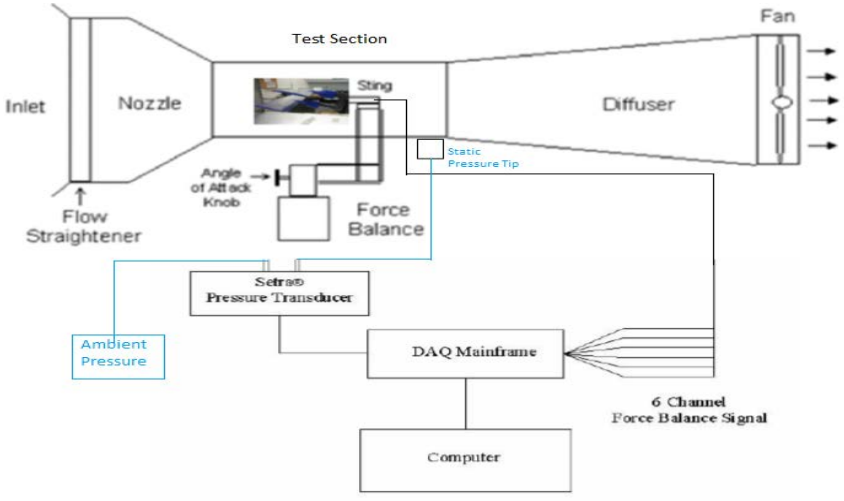

Figure 5. 3: Block Diagram of the Experiment [2].

(d) Experimental Procedure

The experiment procedure was divided in four major sections: Calibration, Single Wing Configurations, various stagger configurations and the flow visualization. The first section was the calibration. The force transducer, Nano 17, was calibrated using 18 point test. The set up for the calibration is shown in figure 5.4. Detailed calibration procedure is provided in appendix C.

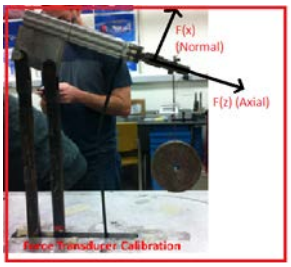

Figure 5.4: Calibration Set Up

Next section was dedicated to obtain normal and axial forces for the single wing configuration. In this section, first the normal and axial force readings with the speed off for angle of attack values of -4, -2, 0, 2, 4, 6, 8, 10, 12, and 14 were recorded as tare weight. Next, the pressure transducers were attached to static pressure taps and other one left open in the air. The pitote tube was not used to measure the speed but the corrections were applied in the calculations. Then, the wind tunnel was set to 15 m/s and data for normal and axial forces were gathered for angle of attack of -4,-2, 0, 2, 4, 6, 8, 10, 12, and 14.

The following section was dedicated to measure the normal and axial forces for different stagger values for the biplane. There 9 different configuration. There were four positive stagger configurations and four negative stagger configurations and one zero stagger configurations. There configurations were adjusted in the PVC pipe test apparatus (figure 5.5). Four different stagger values were as following: 0.25c, .50c, 0.75c and 1.00c, where c is chord length. Then, for each configuration, first the tare weight (normal and axial forces at 0m/s speed) were recorded for angle of attack of -4,-2, 0, 2, 4, 8, 12, and 16 and then the normal and axial forces were recorded for 15m/s and for angle of attack of -4,-2, 0, 2, 4, 8, 12, and 16. All of these data were tabulated according to compare the stagger configurations.

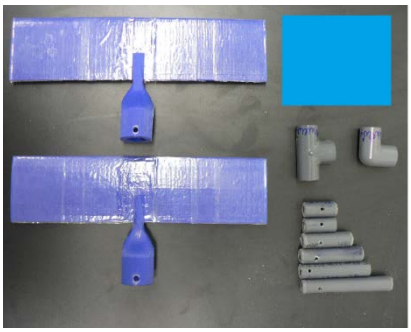
Figure 5.5: Testing Apparatus

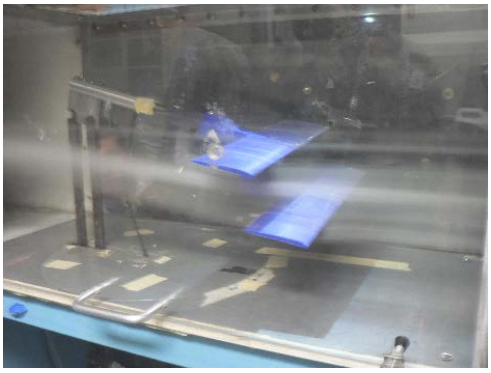
Figure 5. 6: Sample Configuration Set up (-0.25c Stagger)

In the last section, the flow visualization was performed. To visualize the flow, few configurations were chosen. Then using the fog machine and the cardboard box, the streamlines were produced in the test sections. However, due to time limitations in the lab, only couple configurations were used for the flow visualization. All recorded data was connected to check for reasonable results. Once this was affirmed, the experiment was concluded.

6. Results of Experiments

The results are presented in five group of comparison curves. From these curves, the comparison of single airfoil data with Airfoil tools data, single with two airfoils, and different staggers for biplane wings are performed [5]. The accuracy of the results may be inferred from the fact that the deviation of the curve points on the figures from a mean value was within 1-15%. These values can also be seen in Appendix F-1 and Appendix F-2. In investigating and interpreting results, it should be noted that the tests were performed at low Reynolds number of 50,000. It should be also noted that the testing apertures and wing were not elegant, thus it produced large amount of the drag during experiment. In addition, error associated with reading the measurements of the angle of attack is large, since the values were eye-balled by a team member.

(a) Comparison of Single RAF -15 Airfoil with Airfoils Tools data

In this section of the result, the plots for single wing performance were produced to compare with the Airfoils tool's predicted theoretical data. Theoretical data for 2D airfoil obtained from airfoils tools, and experimental data for 2D airfoil and 3D wing were compared in figure 6.1 and figure 6.2. While interpreting the data, it must be noted that the theoretical data from airfoil tools were obtained for Re # of 60,000 [5]. Using equations 1.15, and 1.17, the corrections were applied to 3D experimental data to convert them in 2D airfoil data so it can be compared (see appendix A.4). Induced drag and increased lift slope were observed. The data that was used for plotting these experimental data are presented in appendix F.1.

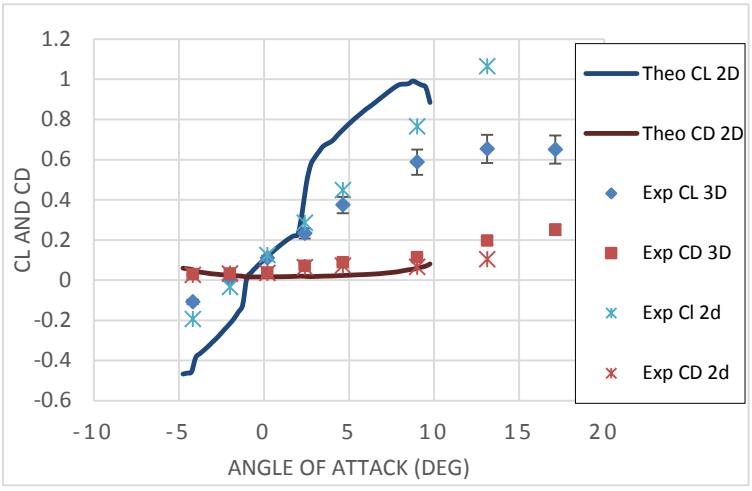

Figure 6. 2: CL and CD vs. Angle of Attack for Single Airfoil

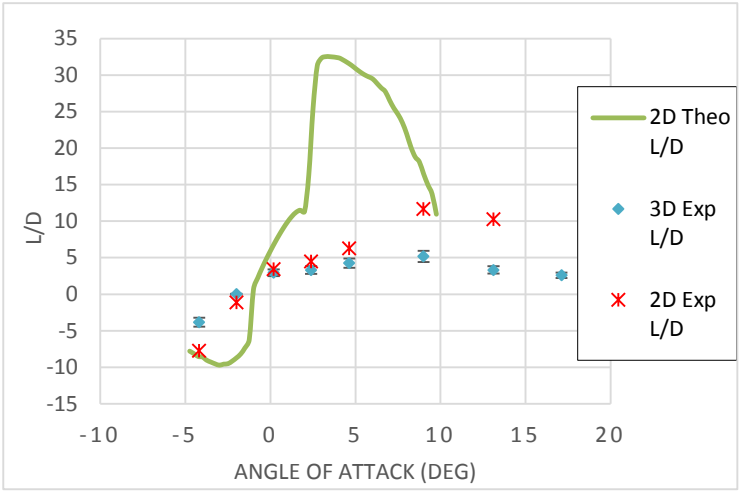

Figure 6. 1: L/D vs. Angle of Attack for Single Airfoil

(b) Comparison of Single RAF-15 Airfoil with Two RAF- 15 Airfoils at Zero S tagger

In this section of the plots (figure 6.3 and 6.4) for CL, CD and lift-drag ratio were produced to compare the aerodynamic forces of single wing and bi plane wings (two wings). The data used for these plots can be obtained from appendix F.1.

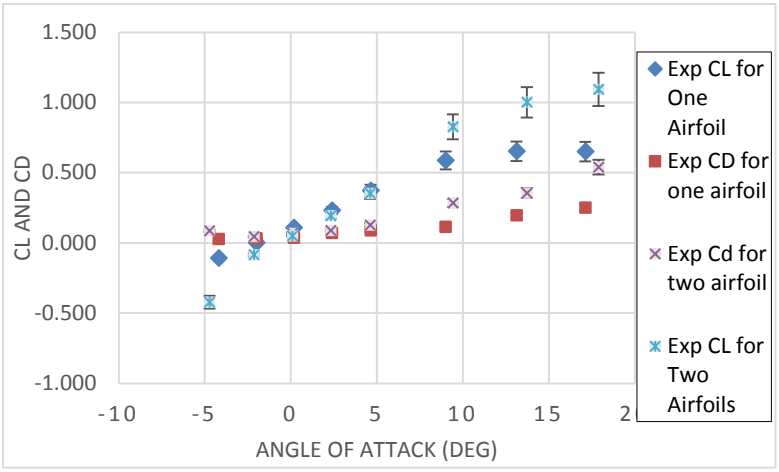

Figure 6.3: CL and CD vs. Angle of Attack for Single and Two Airfoils

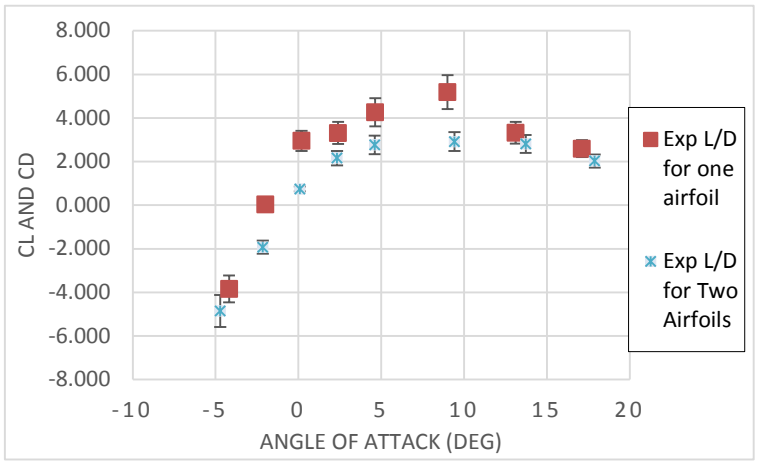

Figure 6. 4: Lift Drag Ratio vs. Angle of Attack for Single and Two Airfoils

(c) Comparison of Lift and Drag for RAF-15 Airfoil with different stagger and at different angle of attack.

In this section, the plot of CL, CD vs. Stagger- Cord Ratio was produced to compare the trends of the coefficient of lift and stagger-cord ratio. It was observed that the lift value for positive stagger compared to negative stagger was larger. The data used for plotting can be obtained from appendix F.2. While interpreting the data, it must be noted that the experimental data from N.A.C.A. were obtained for Re # of 150,000 [3]. In addition, their upper wing was not RAF-15. Instead they used U.S.A 15. However, the gap chord ratio were similar. Note that the values are not compared.

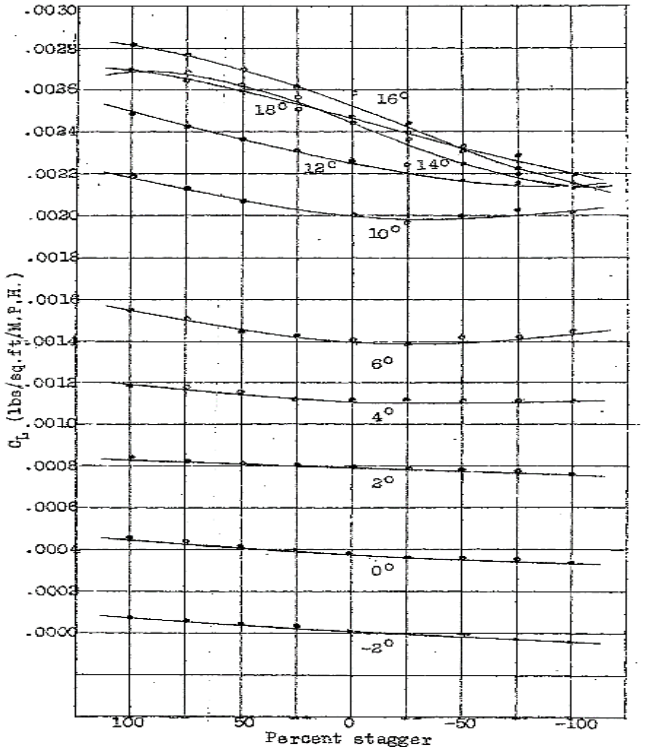

Figure 6.5: CL vs. Angle of Attack for Stagger Comparisons (N.A.C.A Experimental) [3].

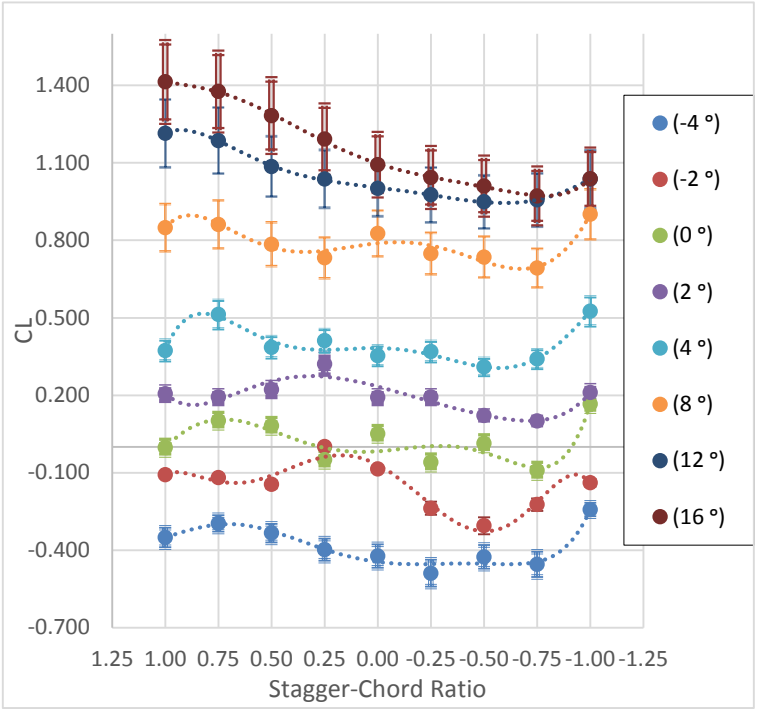

Figure 6.6: CL vs. Angle of Attack for Stagger Comparisons (Experimental)

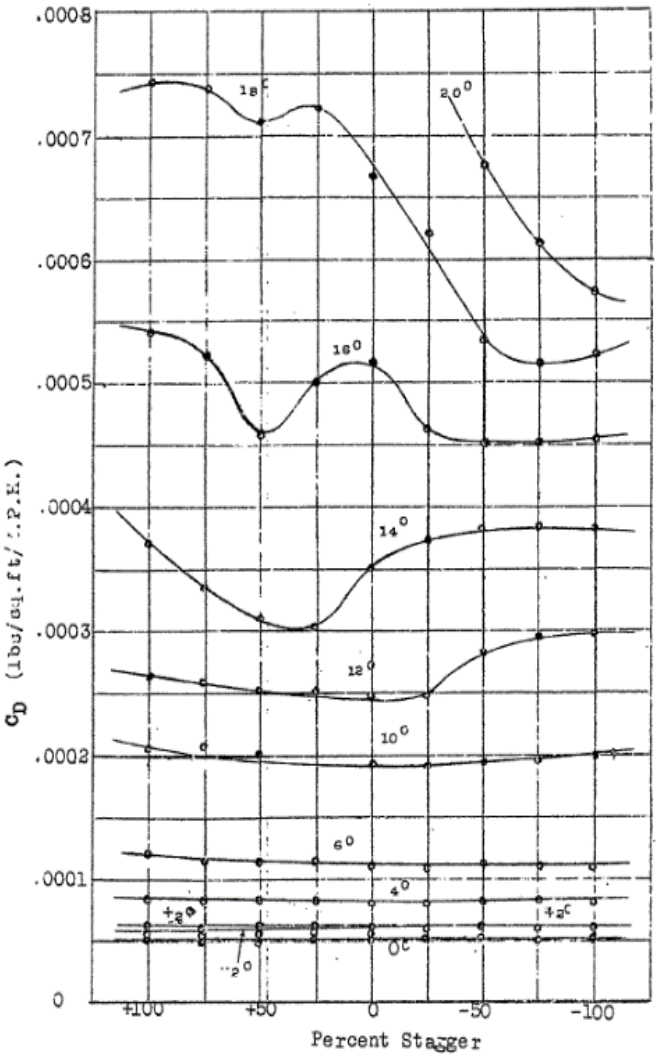

Figure 6. 4: CD vs. Angle of Attack for Stagger Comparisons (N.A.C.A Experimental) [3].

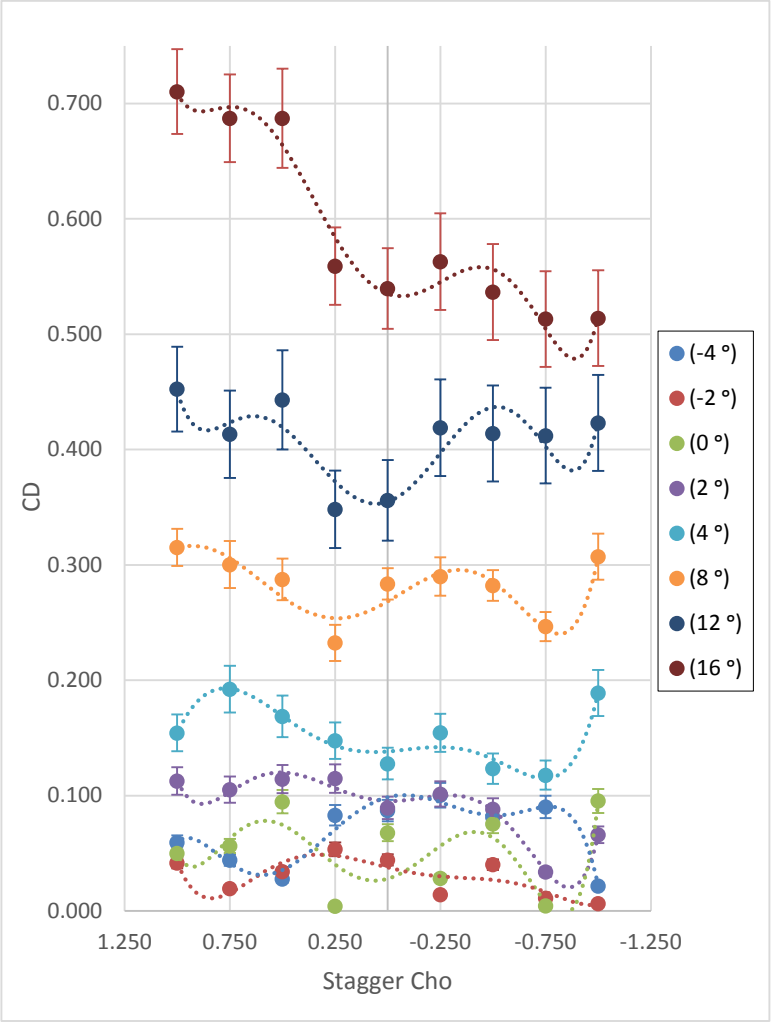

Figure 6. 3: CD vs. Angle of Attack for Stagger Comparisons (Experimental)

(d) Comparison of Lift and Drag for RAF-15 Airfoil with different stagger and at different angle of attack.

In this section, the plot of lift drag ratio vs. stagger- cord ratio was produced to compare the trends of the lift/drag ratio and stagger-cord ratio. While interpreting the data, it must be noted that the theoretical data from N.A.C.A. were obtained for Re # of 150,000 [3]. In addition, the drag values have higher values than actual values due to mounting section of the wing experiences large amount the drag. Only some error bars were shown because they began to make analyzing data harder. In addition, the plot was divided in two figures. Figure 6.10 is for higher positive angles and figure 6.11 is for smaller angle of attack. Some values were ignored and not graphed due to unusual values. These values are available and crossed out in the data in appendix F.2.

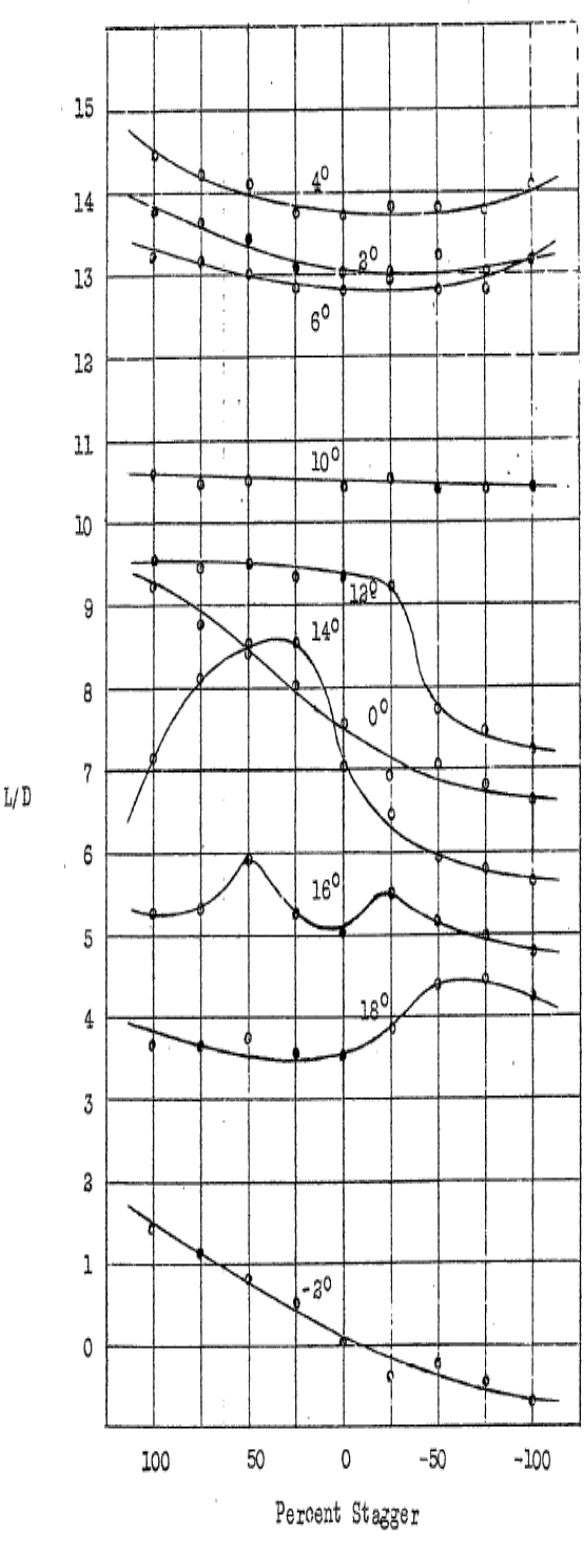

Figure 6. 9: L/D vs. Angle of Attack for Stagger Comparisons (N.A.C.A Experimental) [3].

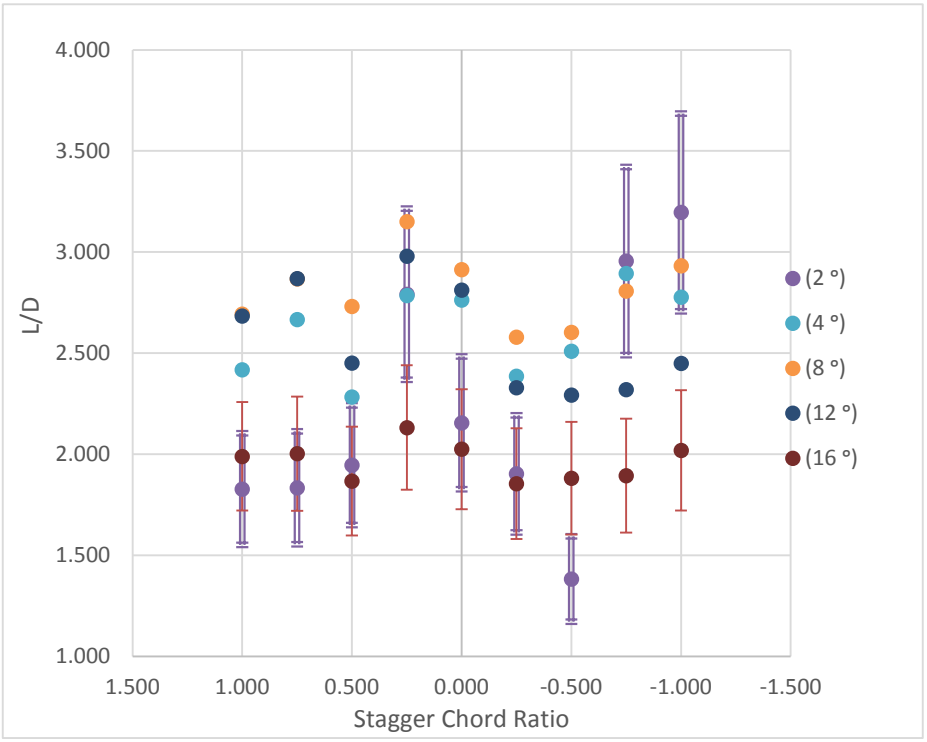

Figure 6. 10: (L/D) vs. Angle of Attack for Stagger Comparisons (High AOA) (Experimental)

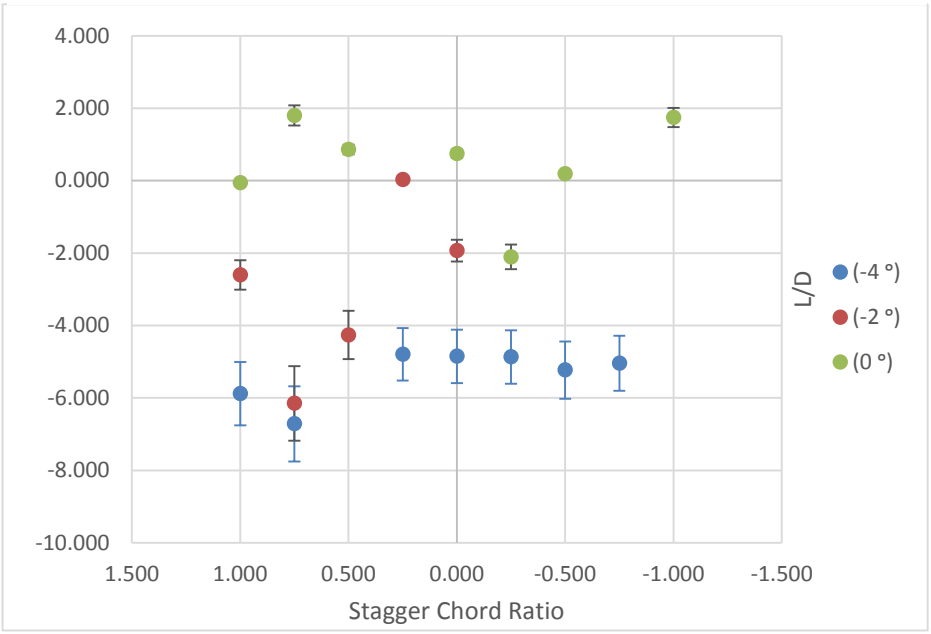

Figure 6. 11: (L/D) vs. Angle of Attack for Stagger Comparisons (Low AOA) (Experimental)

7. Interpretation of Results

(a) Interpretation of Single RAF -15 Airfoil with Airfoils Tools data

From figure 6.1, it can be seen that the lift slope for 3D is smaller compared to 2D lift slope. This is result of vortex flow that wing experiences compared to an airfoil. This vortex flow created induced drag and the actual angle of attack is smaller due to induced angle of attack. These corrections were applied to the 3D experiment data to convert to 2D data. It can be seen that the lift and drag coefficients both followed similar linear and exponential curves as expected. The drag coefficients were higher for the airfoil due to mounting of the airfoil added a large amount of drag that the sting balance measured. Due to these high values, the L/D plot values were little smaller than expected. In addition, the trend for L/D varied a bit as it can be seen in figure 6.2. Theoretical data and experimental data, they both followed the parabolic function but theoretical L/D has a narrow range of parabola compared to experimental. The goal of this comparison was to understand the characteristics of performance of the airfoil.

(b) Interpretation of Single RAF-15 Airfoil with Two RAF- 15 Airfoils at Zero S tagger.

The goal of this comparison was to investigate and compare the RAF 15 wing performance for single wing and biplane wing configuration. According to Anderson, biplane configuration can lift up to 20 percent more than a similarly sized monoplane [1]. This can be seen for higher and lower angles in table 7.1 and figure 6.3, where for the 8 degrees angle of attack there was gain of +0.239 in coefficient of lift in positive stagger compared to negative stagger. They both suggest that the lift will be higher for bi-plane configuration and so is the drag.

		Speed 15/ms and RE # of 50,000									
Angle of Attack (AOA)		Targeted AoA	CL		Gain/Loss for Two Airfoils from One Airfoil	CD		Gain/Loss for Two Airfoils from One Airfoil	L/D		Gain/Loss for Two Airfoils from One Airfoil
One Airfoil	Two Airfoils		One Airfoil	Two Airfoils		One Airfoil	Two Airfoils		One Airfoil	Two Airfoils	
-4.184	-4.720	-4	-0.108	-0.422	-0.314	0.028	0.087	0.059	-3.839	-4.852	-1.013
-1.998	-2.146	-2	0.001	-0.086	-0.087	0.032	0.044	0.012	0.034	-1.932	-1.967
0.187	0.086	0	0.110	0.051	-0.059	0.037	0.068	0.031	2.952	0.745	-2.207
2.396	2.328	2	0.233	0.193	-0.040	0.070	0.089	0.019	3.313	2.155	-1.157
4.637	4.603	4	0.374	0.353	-0.021	0.088	0.128	0.040	4.257	2.764	-1.494
9.002	9.415	8	0.588	0.826	0.239	0.113	0.284	0.170	5.186	2.913	-2.273
13.116	13.718	12	0.653	1.001	0.349	0.196	0.356	0.160	3.327	2.813	-0.514
17.113	17.885	16	0.650	1.093	0.443	0.251	0.540	0.289	2.590	2.025	-0.565

Table 7. 1: Comparison of Single and Two Wings

It can also be seen from table 7.1 and figure 6.3 that the drag is larger for bi plane wing due to two wings experiencing the drag and the structure that is holding the bi plane configuration. For low angle of attack, it was seen that the coefficient of lift decreased for biplane configuration. However, in

theory this cannot be true since both planes are working on the wing and obtains the more lift. This can be also the result that the two wings were at lower angle of attack compared to single wing. In addition, there was a large human error attached to reading the angle of attack.

(c) Interpretation of CL, CD and L/D for Positive and Negative Stagger

In this section, the goal was to compare the wing performance as the stagger values were varied. It can be interpreted from table 7.2 and figures 6.5, 6.7, 6.10 and 6.11 that the positive stagger can provide better performance because there was increase in life but also slight increase in drag for most angles. In addition, these trends were compared with the N.A.C.A results. The values were not compared due to different Aspect Rations and different Reynolds's number that were used during the experiment. For instance, the CL has increased at every target angle for the positive stagger compared to negative stagger. This is the similar trend that is seen for the N.A.C.A report. Similarly, the drag values for experimental results are higher for the positive stagger compare to negative, which can be seen in table 7.2 and figure 6.5. However, the curves were somewhat to theoretical trends from N.A.C.A. These were not similar due to drag that was caused by the mounting mechanism of the wing on the force transducer balance.

	CL Value		CL Increase from Negative to Positive Stagger	CD Value		CD Increase/Decrease from Negative to Positive Stagger	CL Value		L/D Increase from Negative to Positive Stagger
	-0.75 (negative stagger)	+0.75 (positive stagger)		-0.75 (negative stagger)	+0.75 (positive stagger)		-0.75 (negative stagger)	+0.75 (positive stagger)	
(-4 °)	-0.455	-0.296	0.159	0.090	0.044	-0.046	-5.041	-6.716	-1.675
(-2 °)	-0.223	-0.120	0.104	0.011	0.019	0.008	~~-20.012~~	~~-6.148~~	~~13.865~~
(0 °)	-0.092	0.102	0.194	0.005	0.056	0.052	~~-20.317~~	~~1.801~~	~~22.118~~
(2 °)	0.100	0.193	0.093	0.034	0.105	0.071	2.956	1.834	-1.121
(4 °)	0.341	0.513	0.172	0.118	0.192	0.075	2.895	2.667	-0.228
(8 °)	0.692	0.861	0.169	0.247	0.300	0.054	2.807	2.868	0.061
(12 °)	0.956	1.186	0.230	0.412	0.413	0.001	2.321	2.870	0.549
(16 °)	0.972	1.376	0.404	0.513	0.687	0.174	1.894	2.003	0.109

Table 7. 1: Comparison for Performance at various Staggers

Furthermore,. It can be interpreted from table 7.2 and figure 6.10 and 6.11 that the Lift and Drag ratio was negative for lower angles and positive for higher angle for positive stagger compared to negative stagger. This was not similar to N.A.C.A results. N.A.C.A experimental results suggest that the lift and drag ratios are better for the positive staggers compared to negative stagger for most of the angle of attack. One similar trend that was observed was in the experiment and N.A.C.A experiment the value of Lift Drag ratio first increased and then decreased with the angle of attack. These trends care seen in figure 6.10 and figure 6.11.

(d) Flow Visualization and its interpretation.

After all the data collections and plotting, the flow visualization was performed using fog machine to visualize the flow characteristics on the airfoil. The positive staggered flow visualization is shown in figure 7.1 and the negative staggered flow visualization is shown in figure 7.2. It was observed that the airfoil experienced a large amount of drag on the mounting position where it separated the most. In addition, it was observed that the flow due to lower wing in negative stagger configuration affected the flow that the upper wing experienced. This might have led to decreased lift and decreased drag compared to positive staggered configuration. In the positive stagger configuration, the flow that created lift on lower wing was affected very little due to upper wing, it may have been the reason of higher lift and higher drag in the positive staggered configuration.

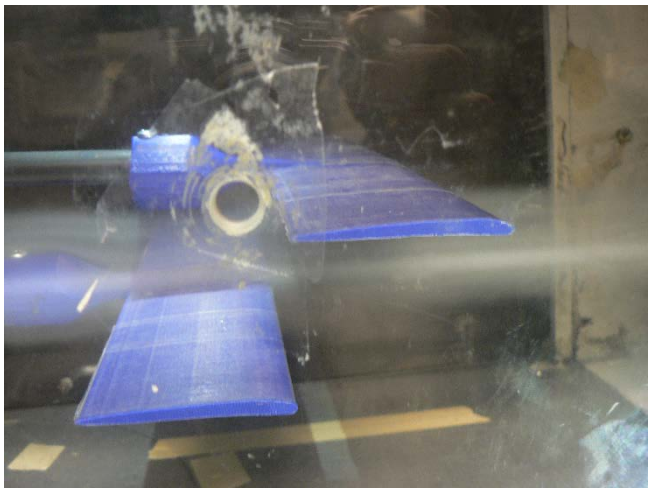

Figure 7. 1: Flow Visualization for Positive Stagger Configuration.

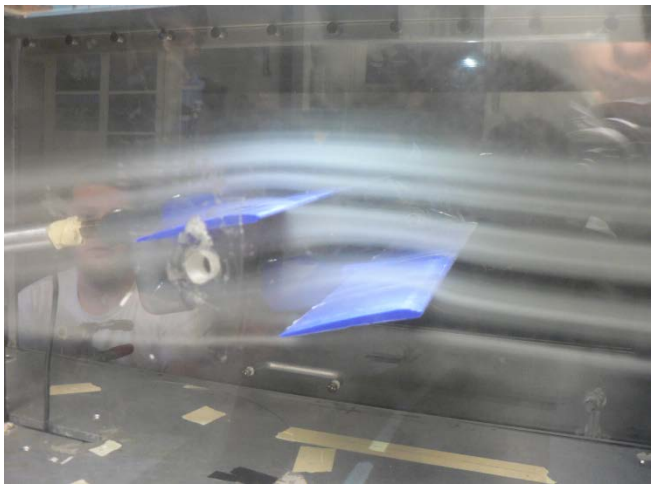

Figure 7. 2: Flow Visualization for Negative Stagger Configuration.

8. Conclusions

The experiment was performed to measure the Lift, Drag, and Lift-Drag ratio of a R.A.F airfoil in single wing, bi plane wings, and various stagger configurations while varying the angle of attack. First conclusion that was made that the biplane wing provided higher lift at the cost of higher drag. However, the lift and drag ratio was lower for biplane configuration. This was the result of increased drag due to structure and the mounting mechanism of the airfoil. With the two wings, the lift is not doubled and the drag is increased little more because both wings has a little room to work on available fluid. Furthermore, positive staggered configuration obtained higher lift and drag compared to negative staggered configuration. In conclusion, the positive stagger for biplanes have advantage because it increases lift and has advantage of vision to pilot in cockpit.

9. Sources of Errors

In the experiment, there were three major source of error, which may have led to errors that are associated with the experiment. First major source was the testing apparatus. The mounting mechanism (see figure 5.5) created a large amount of drag due to flow separation around the back cylinder. This added up in the total and drag and it affected the Lift Drag ratio which resulted in different than the N.A.C.A experimental data and Airfoil tool's xfoil prediction.

Second major source of error was the method that was used to measure the angle of attack. This measurement was eye-balled by team member. There was a difficulty in reading the angle of attack because it was measured from far and outside the test section. Most of the calculations were based on this angle of attack measurements. As a result, there is an error attached to the data that was gathered and calculated in this experiment.

Furthermore, the third major source of error was that minor vibrations and fluctuations were observed in the force transducers were observed. Since the data was averaged out across 1000 points, these vibrations were included in the experiment data. In short, if these error can be corrected, then the experiment ma provide better results. Recommendations are provided in the following section.

10. Recommendations

As has been mentioned, there were few major errors associated in the method that this experiment was conducted. For future experiment, there are few methods that can be used for better results. First recommendation is to use different, big and clean wind tunnel for better visual effects and if done so, then the wall effects can be ignored. Second recommendation is to produce better wing structure and mounting mechanism. As a result, drag measured will be close to actual drag values. In addition, develop better and rigid structure for different staggered configurations for better alignments. Other recommendation is to develop better method of recording angle of attack, so it provides performance values that are closer to actual values. Furthermore, vibrations can be corrected if more data are taken and using statistical data, the outliers should be taken out for each measurements. Next recommendation is to repeat the process of taking measurement at single point multiple times. In addition, the experiment should be conducted through more and smaller interval of angle of attack. This will provide more in depth analysis and transitions can be analyzed with more details. All of these recommendations may result in better results; therefore they should be considered for similar future experiment.

11. Acknowledgments

I would like to express my deepest appreciation to Professor Manuel Gamero Castano who provided me the possibility to complete this experiment and report. Many thanks to him for providing me with the technical and non-technical lectures on the subject matters of the experiment. It would not have been possible without the kind support and help of many individuals. I would like to extend my sincere thanks to all of them.

I am highly indebted to Rayomand Gundevia for his guidance and constant supervision as well as for providing necessary information regarding the experiment & also for his support in completing the experiment. I would also like to thank Alejandro Puga for helping us with the pre-lab procedures and guidance for preparations for the lab periods. My thanks and appreciations also go to my colleague in developing the project and people who have willingly helped me out with their abilities.

Special thanks to the Henry Samuli School of Engineering and the mechanical and aerospace department for allowing MAE 108 students to use the wind tunnel facility for their design experiment.

12. List of References

[1] J. D. Anderson. *Fundamentals of Aerodynamics,* 3rd edition, McGraw-Hill Companies, 2001

[2] John LaRue. “MAE 108 Aerospace Laboratory Manual.” University of California, Irvine. 2009. 27 Oct. 2013.

[3] F.H. Norton at el. “THE EFFECT OF STAGGERING A BIPLANE”. *National Advisory Committee for Aeronautics*. Report No. 70. September, 1921. 10 Oct. 2013.

[4] Montgomery Knight and Richard W. Noyes. “Wind Tunnel Pressure Distribution Tests on a series of biplane wing models.” *National Advisory Committee for Aeronautics*. Report No. 330. December, 1929. 10 Oct. 2013.

[5] “RAF 15 AIRFOIL” Airfoil Tools. *AirfoilTools.com*. 2013. 10 Oct. 2013.

[6] Tim Brice and Todd Hall. The Weather Calculator. National Weather Services. *USA.gov.* 1 Oct. 2009. 10 Oct. 2013.

[7] Specifications of Nano17. *ATI Industrial Automation.* 2013. 1 Oct. 2009. 10 Oct. 2013.

Appendices

Appendix A: Method Used for Calculations

This section explains what approach and equations were used during the experiment such as calculations for density, lift, drag and corrections. It assumes that basic equations are known and therefore they are not shown in the report. All the units for the variables and the constants used are in SI unit system. These methods and equations were used in the theoretical presentations as well. It explains how the wall effects were integrated in the data of the report. Subsections of these sections are as following:

A. 1 - Method of Calculating Density

A. 2 - Method of Calculating Aerodynamic Forces and Coefficients

A. 3 - Wall Effect Corrections

A. 4 - 3D Correction in order to compare to 2D.

A.1 Method to Calculate Density:

All of equations for A.1were obtained from National Weather Service [6].

Using equations 1.1, 1.2, 1.3 it was determined that the equation 1.4 can be used to calculate the density of humid air.

$$p_v = \phi p_{\text{sat}} \text{..... [Eqn 1.1]}$$

$$p_d = p - p_v \text{..... [Eqn 1.2]}$$

$$p_{\text{sat}} = 6.1078 \times 10^{\frac{7.5T}{T+237.3}} \text{..... [Eqn 1.3]}$$

$$\rho_{\text{humid air}} = \frac{p_d}{R_d T} + \frac{p_v}{R_v T} \text{..... [Eqn 1.4]}$$

Legend:

p_d =Partial pressure of dry air (Pa)

R_d = Specific gas constant for dry air, 287.058 J / (kg•K)

T = Temperature (K)

p_v = Pressure of water vapor (Pa)

R_v = Specific gas constant for water vapor, 461.495 J/ (kg•K)

p = Relative humidity

p_v = Saturation vapor pressure (Pa)

A.2 Method to Calculate Aerodynamic Forces and Coefficients:

Equations/Image obtained for this method were obtained from Anderson's Book [1].

1) Normal and Axial Force
    a. These forces were obtained using the F/T Sensor: Nano17 [7].
2) Lift and Drag and Axial Force
    a. Using the 3rd axis rotation matrix, Lift and Drag forces were obtained from normal and axial forces.

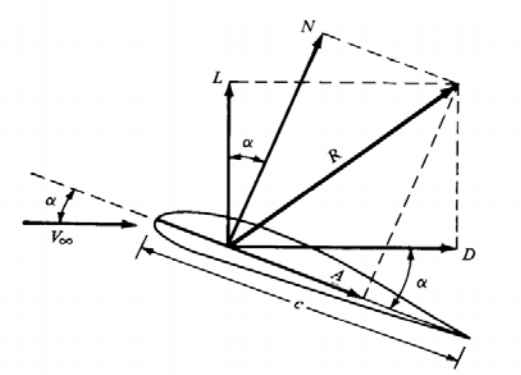

Figure A.2.1: Reference Frame for Lift and Drag [1].

$$F_L = F_N \cos(\alpha) - F_a \sin(\alpha) \ldots\ldots \text{[Eqn 1.5]}$$

$$F_D = F_a \cos(\alpha) + F_N \sin(\alpha) \ldots\ldots \text{[Eqn 1.6]}$$

$Where,\ F_L$ = Lift Force, F_D = Drag Force, F_N = Normal Force, F_a = Axial Force, $\alpha - angle\ of\ attack$

3) Lift and Drag Coefficient
    a. Using Equations 2.1 and 2.2 and dimensionless analysis, the lift and drag were made dimensionless as following.

$$q_\infty = \frac{1}{2}\rho V_\infty^2 \ldots\ldots \text{[Eqn 1.7]}$$

$$V = \sqrt{\left(\frac{2 * \Delta P}{\rho}\right)} \ldots. \text{[Eqn 1.8]}$$

$$C_L = \frac{F_L}{q_\infty * c * s} \ldots\ldots \text{[Eqn 1.9]}$$

$$C_D = \frac{F_D}{q_\infty * c * s} \ldots\ldots \text{[Eqn 1.10]}$$

$Where, \rho_\infty$ = Free Stream Density, V_∞ = Free Stream Velocity q_∞

q_∞ = Dynamic pressure, c = cord, $s - span$

4) Lift and Drag Ratio:
    a. From equations 2.4 and 2.5, the lift and drag ratio was obtained.

$$\frac{L}{D} = \frac{C_L}{C_D} \ldots\ldots \text{[Eqn 1.11]}$$

A.3 Method to Integrating Wall Effects

Equations obtained for this method were obtained from MAE 108 Lab manual [2].

The volume of air inside the test section of the wind tunnel is confined; therefore, it is necessary to apply wall effects to the angle of attack, aerodynamic coefficients. This corrections are applied to data in order to correct the wind tunnel data so it can be consistent with measurements made in an unconfined volume. The additive corrections that were applied to data are as following:

$$\Delta\alpha = 1.7 * C_L \quad \text{…….. [Eqn 1.12]}$$

$$\Delta C_D = 0.03 * C_L^2 \text{…… [Eqn 1.13]}$$

A.4 3D Corrections:

(a) Equations used

$$a = \frac{a_0}{\left(1+\frac{a_0}{\pi * e * AR}\right)} \ldots \text{[Eqn 1.14]}$$

$$a_o = \frac{a}{\left(1-\frac{a}{\pi * e * AR}\right)} \ldots \text{[Eqn 1.15]}$$

$$CD_i = \frac{CL^2}{\pi e AR} \ldots \text{[Eqn 1.16]}$$

$$CD = CD_{3d} - CD_i \ldots \text{[Eqn 1.17]}$$

Where a = the lift slop for 3D wing

ao = the lift slop for 2D wing

e = wind efficiency (assumed to be 0.95)

AR = Aspect Ratio (4.1 for this wing)

CDi = Induced Drag due to vortices.

(b) Method and the Plots used.

Using excel, the lift slope of single wing was obtained from the plots that can be seen below. Using equation 1.15, 1.16, and 1.17. The corrections were applied. Corrected values were plotted and the data for corrected values are in appendix F.1.

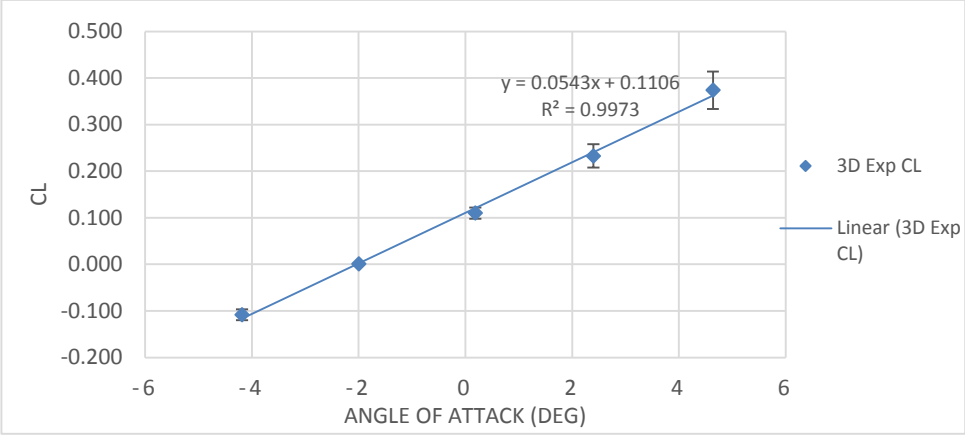

Figure A.4.1: 3D Corrections

AR	4.109589
e	0.95
a / deg	0.0543
a / rad	3.111161
a0 / rad	4.168552
ao / deg	0.072755
y int	0.1106

Appendix B: Uncertainty Analysis

This section provides value and equations for associated error with the experiment. The errors associated with the instrument used in the experiment can be obtained in this section. Error refers only to the uncertainty in our result, regardless of what the expected value is supposed to be. It also shows how the error analysis was derived and performed.

B. 1 - Instrument Errors Obtained / Measured / Given

B. 2 - Derivations for the Error Associated in Aerodynamic Forces and Coefficients

B.1 Instrument Errors Obtained / Measured / Given

Constants	
Measurement Device	Precision
Length (m) - Calipers	0.0050
Angle (Deg) - Level	0.0500
Angle (rad)	0.0009
Pressure Transducers (Pa)	0.5600
F/T Sensor: Nano17 / Balance Precision Force (N) [7]	0.0028
F/T Sensor: Nano17 / Balance Precision Torque (Nm) [7]	1.6E-05

Table B.1.1: Instrument Uncertainty

B.2 Derivations for the Error Associated in Aerodynamic Forces and Coefficients

- The following techniques are used to determine how error propagates through an experimental procedure.

I. $A = c * s$ ….. $[Eqn\ 1.18]$ $===>$ $\delta A = \delta c * s + \delta s * c$ … ….[Eqn 1.19]

II. $q_\infty = \frac{1}{2}\rho V_\infty^2$ $====>$ $\delta q_\infty = \rho * V * \delta V$ ….[Eqn 1.16]

III. $V = \sqrt{\left(\frac{2*\Delta P}{\rho}\right)}$ …. $=>$ $\delta V = \sqrt{\frac{2}{\rho}} * \left(\frac{1}{2}\right) * \left(\Delta P^{-\frac{1}{2}}\right) * \delta\Delta P = \sqrt{\frac{1}{2\rho\Delta P}}\ \delta\Delta P$ ….[Eqn 1.20]

IV. $L = F_n \cos(\alpha) - F_a \sin(\alpha)$

$$\delta L = \cos(\alpha) * \delta F_n - F_n\ (\sin(\alpha))\delta\alpha - \sin(\alpha) * \delta F_a - F_a\ (\cos(\alpha))\delta\alpha$$

$\delta L = \sqrt{(\cos^2(\alpha) * \delta F_n^2) + (F_n^2\ (\sin^2(\alpha))\delta\alpha^2) + (\sin^2(\alpha) * \delta F_a^2) + (F_a^2(\cos^2(\alpha))\delta\alpha^2)}$ ….[Eqn 1.21]

V. $D = F_a \cos(\alpha) + F_n \sin(\alpha)$

$$\delta D = \cos(\alpha) * \delta F_a - F_a\ (\sin(\alpha))\delta\alpha + \sin(\alpha) * \delta F_n + F_n\ (\cos(\alpha))\delta\alpha$$

$\delta D = \sqrt{(\cos^2(\alpha) * \delta F_a^2) + (F_a^2\ (\sin^2(\alpha))\delta\alpha^2) + (\sin^2(\alpha) * \delta F_n^2) + (F_n^2(\cos^2(\alpha))\delta\alpha^2)}$ ….[Eqn 1.22]

VI. $C_L = \frac{L}{q_\infty * A}$ $===>$ $\delta C_L = \left(\frac{1}{q_\infty * A}\delta L\right) - \left(\frac{L}{q_\infty^2 A}\delta q_\infty\right) - \left(\frac{L}{q_\infty * A^2}\delta A\right)$

$$\sqrt{(\delta C_L)^2} = \sqrt{\left(\frac{1}{q_\infty^2 * A^2}\delta L^2\right) + \left(\frac{L^2}{q_\infty^4 A^2}\delta q_\infty^2\right) + \left(\frac{L^2}{q_\infty^2 * A^4}\delta A^2\right)}$$ ….[Eqn 1.23]

Similarly,

VII. $\delta C_D = \sqrt{\left(\frac{1}{q_\infty^2 * A^2}\delta D^2\right) + \left(\frac{D^2}{q_\infty^4 A^2}\delta q_\infty^2\right) + \left(\frac{D^2}{q_\infty^2 * A^4}\delta A^2\right)}$ ….[Eqn 1.24]

VIII. $\frac{L}{D} = \frac{C_L}{C_D}$ ….[Eqn 1.25]

$$\delta\left(\frac{L}{D}\right) = \left(\frac{(C_D * \delta C_L) - (C_L * \delta C_D)}{C_D^2}\right) = \frac{1}{C_D}\delta C_L - \left(\frac{C_L}{C_D^2}\right)\delta C_D$$

$$\delta\left(\frac{L}{D}\right) = \sqrt{\left(\frac{1}{C_D}\delta C_L\right)^2 + \left(\left(\frac{C_L}{C_D^2}\right)\delta C_D\right)^2}$$ [Eqn 1.26]

Appendix C: Calibration

This section provides the data tables, calculations and the charts that were used during calibration of the F/T Sensor: Nano17. Different mass and different position on the shaft were recorded, then the applied and measured values were plotted to visualize the calibration of the F/T Sensor: Nano17.

C. 1 - Detailed Procedure of the Calibration

C. 2 - Data/Calculations/Charts used for Calibration Purposed.

C.1 Detailed Calibration Procedure

Before turning the wind tunnel on, the LabView software was calibrated by setting the offset to zero and gain to one in the horizontal position. The first measurements were taken to clear the initial offset values for the following experiments. The mean of each force (3 axes) and torque readings were applied as the offset, except for Ty, with no object placed on the sting arm. A measurement was run to verify zero readings.

To calibrate the device, 18 different configurations of known applied values were choose. For these configurations, 3 different mass, 3 different angles and 2 different positions were chosen. The axis of the balance is shown below.

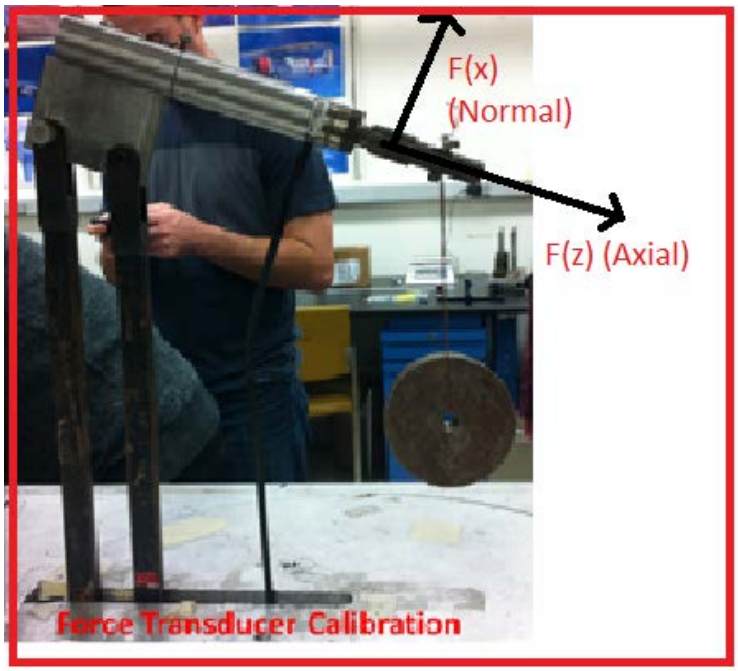

Figure C.1.1: Calibration Set Up for the Experiment

Then, the excel spreadsheets were produced to compare and the plot the values to redo points if they differ by great amount. Using Lab view software, the force values were calculated and plotted in the excel. The actual applied vs. the measured forces, and applied vs. measured torques were plotted. The correlation was found to be close to 1:1. This slope of correlation was representing the gain value in the software. The force balance was confirmed to be accurate with an 18 point test within the desired range;

C.2 Calibration information for equipment and sensors

m (kg)	F (N)	Position (mm)	Position adjusted to center of torque	angle (Deg)	Fx (N)		Fz (N)		Ty (Nmm)		
					applied	measured	applied	measured	applied	measured	Adjusted
0.041	0.402	108.4	37.4	-0.3	-0.402	-0.397	-0.002	0.057	-15.038	-7.713	4.287
0.041	0.402	79.4	8.4	-0.3	-0.402	-0.406	-0.002	0.009	-3.378	3.893	15.893
0.197	1.932	108.4	37.4	-0.3	-1.932	-1.935	-0.010	0.112	-72.256	-61.411	-49.411
0.197	1.932	79.4	8.4	-0.3	-1.932	-1.942	-0.010	0.069	-16.229	-9.466	2.534
0.390	3.825	108.4	37.4	-0.3	-3.825	-3.834	-0.020	0.201	-143.045	-130.773	-118.773
0.390	3.825	79.4	8.4	-0.3	-3.825	-3.833	-0.020	0.142	-32.128	-25.418	-13.418
0.041	0.402	110.8	39.8	12.8	-0.392	-0.398	-0.089	-0.058	-16.003	-7.804	-7.804
0.041	0.402	76.2	5.2	12.8	-0.392	-0.397	-0.089	-0.086	-2.091	4.949	4.949
0.197	1.932	110.8	39.8	12.8	-1.884	-1.894	-0.428	-0.356	-76.893	-67.252	-67.252
0.197	1.932	76.2	5.2	12.8	-1.884	-1.899	-0.428	-0.380	-10.046	-4.132	-4.132
0.390	3.825	110.8	39.8	12.8	-3.730	-3.746	-0.847	-0.701	-152.224	-141.458	-141.458
0.390	3.825	76.2	5.2	12.8	-3.730	-3.704	-0.847	-0.805	-19.889	-14.755	-14.755
0.041	0.402	108.4	37.4	-12.9	-0.392	-0.394	0.090	0.098	-15.038	-7.267	-7.267
0.041	0.402	79.4	8.4	-12.9	-0.392	-0.389	0.090	0.076	-3.378	3.682	3.682
0.197	1.932	108.4	37.4	-12.9	-1.883	-1.894	0.431	0.473	-72.256	-63.381	-63.381
0.197	1.932	79.4	8.4	-12.9	-1.883	-1.898	0.431	0.418	-16.229	-9.871	-9.871
0.390	3.825	108.4	37.4	-12.9	-3.728	-3.744	0.854	0.940	-143.045	-131.175	-131.175
0.390	3.825	79.4	8.4	-12.9	-3.728	-3.750	0.854	0.840	-32.128	-24.308	-24.308

Table C.2.2: Force Transducer Calibration Data

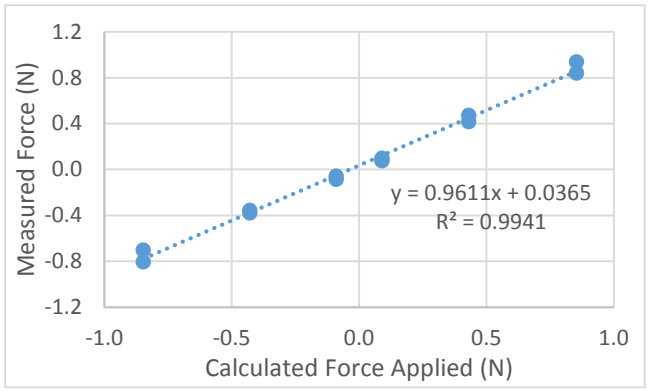

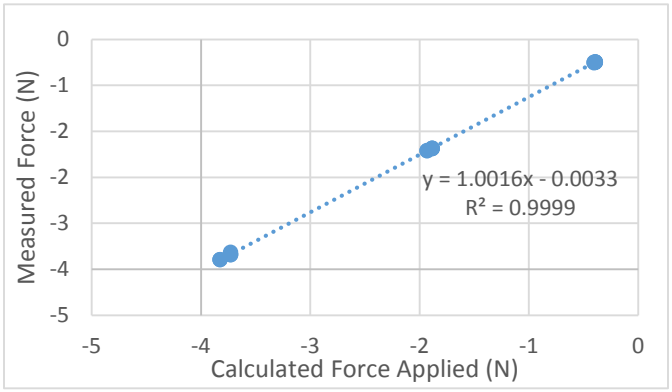

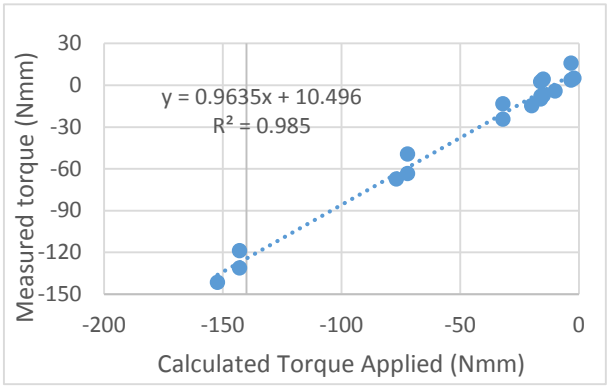

Figure C.1.1: Plots Used for Calibration

Appendix D: Trend Lines

This section shows the table of the trend lines that were fitted to CL vs. Stagger Chord Ratio and CD vs. Stagger Chord Ratio.

D.1 Tabulated Trend Line Equations.

In this section, the trend lines equations are presented that were obtained from applying 6th degree polynomial fit in excel to points in order to analyze and visualize basic trends.

Angle of Attack (Deg)	CL (y) vs. Stagger Chord Ratio (x)
16	$y = 0.269x^6 - 0.171x^5 - 0.437x^4 + 0.088x^3 + 0.296x^2 + 0.272x + 1.0975$
12	$y = -0.250x^6 - 0.235x^5 - 0.398x^4 + 0.224x^3 + 0.027x^2 + 0.101x + 1.005$
8	$y = -0.388x^6 - 0.658x^5 + 0.834x^4 + 0.715x^3 - 0.361x^2 - 0.0827x + 0.789$
4	$y = -0.721x^6 - 0.5957x^5 + 1.114x^4 + 0.5125x^3 - 0.326x^2 - 0.0082x + 0.383$
2	$y = 0.3497x^6 + 0.167x^5 - 0.230x^4 - 0.385x^3 - 0.144x^2 - 0.217x + 0.2336$
0	$y = 0.5592x^6 - 0.8021x^5 - 0.7702x^4 + 0.777x^3 + 0.3087x^2 - 0.0592x + 0.017$
-2	$y = -1.363x^6 + 0.581x^5 + 2.426x^4 - 0.9903x^3 - 1.1182x^2 + 0.4269x - 0.0698$
-4	$y = 0.4672x^6 - 0.3252x^5 - 0.685x^4 + 0.168x^3 + 0.367x^2 + 0.1046x - 0.445$

Table D.1.3: 6 Degree Polynomial Trend line fit for CL vs. Stagger Chord Ratio.

Angle of Attack (Deg)	CD (y) vs. Stagger Chord Ratio (x)
16	$y = 0.6612x^6 - 0.184x^5 - 1.1239x^4 + 0.2152x^3 + 0.5397x^2 + 0.0655x + 0.5351$
12	$y = 0.7476x^6 - 0.1367x^5 - 1.215x^4 + 0.211x^3 + 0.550x^2 + 0.0615x + 0.355$
8	$y = 0.2179x^6 - 0.3461x^5 - 0.2708x^4 + 0.4548x^3 + 0.0954x^2 - 0.1053x + 0.268$
4	$y = 0.1061x^6 - 0.2755x^5 - 0.1521x^4 + 0.2713x^3 + 0.0795x^2 - 0.0134x + 0.1383$
2	$y = 0.4677x^6 + 0.122x^5 - 0.637x^4 - 0.140x^3 - 0.163x^2 - 0.0053x + 0.0954$
0	$y = 0.746x^6 - 0.293x^5 - 1.094x^4 + 0.321x^3 + 0.3921x^2 - 0.0509x + 0.00279$
-2	$y = -0.422x^6 + 0.0945x^5 + 0.661x^4 - 0.029x^3 - 0.296x^2 - 0.046x - 0.0985$
-4	$y = 0.1853x^6 + 0.124x^5 - 0.2382x^4 + 0.151x^3 + 0.0337x^2 + 0.0451x + 0.0378$

Table D.1.2: 6 Degree Polynomial Trend line fit for CD vs. Stagger Chord Ratio.

Appendix E: Programs Used

This section describes what softwares were used for obtaining data and performing calculations. The major components and what were these software were used for is also described in this appendix.

E. 1 - LabView – Used with the instruments to Obtain Values

E. 2 - Excel – It was used to create Data tables, calculate desired values, and graph the desired results.

E.1 LabView

LabView was used to calibrate the F/T: Nano 17 and it was used to obtain the normal forces and axial forces experienced by the wings. This also provided the values for velocities and dynamic pressure. The dynamic pressure obtained from this was from pressure transducers attached to static ports of the wind tunnel. These were calculated later using the Pitote tube correction.

E.2 Excel

Excel was used to tabulate all the recorded data. Then it was used for desired calculations. It made it easier for recording and visualizing a large amount of data. These data and calculations were tabulated and graphed using excel as well.

Appendix F: Tabulated Data / Spreadsheets

This section is to provide all the data that was collected and tabulated for the experiment.

F. 1 - Data Tables for Single Wing and Two Wing (@ 0 Stagger)

F. 2 - Data Tables used to Compare Staggers at Different Angles.

F. 3 - Filled Spreadsheets

F. 4 - Sample Spreadsheets (Method used in Tabulating and Calculating)

F.1 Data Tables for Single Wing and Two Wing (@ 0 Stagger)

Single Airfoil @ 15 m/s => RE# = 50,000										
Angle of Attack (Deg)	**CL**	**δCL**	**2D CL**	**CD**	**δCD**	**Induced CD**	**2D CD**	**L/D**	**δ(L/D)**	**2D L/D**
-4.184	-0.108	0.012	-0.194	0.028	0.003	0.003	0.025	-3.839	0.614	-7.726
-1.998	0.001	0.001	-0.035	0.032	0.004	0.000	0.032	0.034	0.044	-1.090
0.187	0.110	0.012	0.124	0.037	0.004	0.001	0.036	2.952	0.461	3.452
2.396	0.233	0.025	0.285	0.070	0.008	0.007	0.064	3.313	0.506	4.480
4.637	0.374	0.040	0.448	0.088	0.009	0.016	0.071	4.257	0.646	6.270
9.002	0.588	0.063	0.766	0.113	0.012	0.048	0.066	5.186	0.776	11.686
13.116	0.653	0.070	1.065	0.196	0.020	0.092	0.104	3.327	0.498	10.262
17.113	0.650	0.070	-	0.251	0.026	-		2.590	0.389	

Two Airfoils @ 15 m/s => RE# = 50,000						
Angle of Attack (Deg)	**CL**	**δCL**	**CD**	**δCD**	**L/D**	**δ(L/D)**
-4.720	-0.422	0.045	0.087	0.009	-4.852	0.735207
-2.146	-0.086	0.009	0.044	0.005	-1.932	0.300336
0.086	0.051	0.006	0.068	0.007	0.745	0.115628
2.328	0.193	0.021	0.089	0.010	2.155	0.328171
4.603	0.353	0.038	0.128	0.014	2.764	0.41899
9.415	0.826	0.089	0.284	0.029	2.913	0.431657
13.718	1.001	0.108	0.356	0.035	2.813	0.409894
17.885	1.093	0.119	0.540	0.053	2.025	0.29665

F.2 Data Tables used to Compare Staggers at Different Angles.

(-4 °)						
Stagger	CL	δCL	CD	δCD	**L/D**	**δ(L/D)**
0.000	-0.422	0.045	0.087	0.009	-4.852	0.735
-0.250	-0.489	0.052	0.100	0.011	-4.870	0.735
-0.500	-0.426	0.046	0.081	0.009	-5.230	0.793
-0.750	-0.455	0.049	0.090	0.010	-5.041	0.762
-1.000	-0.243	0.026	0.022	0.003	-11.226	1.858
0.250	-0.398	0.043	0.083	0.009	-4.794	0.727
0.500	-0.334	0.036	0.028	0.003	-12.060	1.910
0.750	-0.296	0.032	0.044	0.005	-6.716	1.036
1.000	-0.350	0.038	0.060	0.006	-5.883	0.872

(4 °)						
Stagger	CL	δCL	CD	δCD	**L/D**	**δ(L/D)**
0.000	0.353	0.038	0.128	0.014	2.764	0.419
-0.250	0.369	0.040	0.155	0.017	2.386	0.362
-0.500	0.310	0.033	0.123	0.013	2.510	0.381
-0.750	0.341	0.037	0.118	0.013	2.895	0.439
-1.000	0.525	0.056	0.189	0.020	2.778	0.419
0.250	0.411	0.044	0.148	0.016	2.785	0.422
0.500	0.386	0.041	0.169	0.018	2.284	0.346
0.750	0.513	0.055	0.192	0.020	2.667	0.403
1.000	0.373	0.040	0.154	0.016	2.418	0.362

(-2 °)						
Stagger	CL	δCL	CD	δCD	**L/D**	**δ(L/D)**
0.000	-0.086	0.009	0.044	0.005	-1.932	0.300
-0.250	-0.238	0.025	0.014	0.002	-16.738	3.027
-0.500	-0.305	0.033	0.040	0.005	-7.594	1.178
-0.750	-0.223	0.024	0.011	0.002	-20.012	3.921
-1.000	-0.139	0.015	0.006	0.002	-21.422	5.790
0.250	0.002	0.001	0.053	0.006	0.029	0.026
0.500	-0.145	0.016	0.034	0.004	-4.261	0.667
0.750	-0.120	0.013	0.019	0.002	-6.148	1.029
1.000	-0.108	0.012	0.042	0.005	-2.604	0.403

(8 °)						
Stagger	CL	δCL	CD	δCD	**L/D**	**δ(L/D)**
0.000	0.826	0.089	0.284	0.029	2.913	0.432
-0.250	0.748	0.081	0.290	0.030	2.580	0.386
-0.500	0.735	0.079	0.282	0.029	2.603	0.389
-0.750	0.692	0.075	0.247	0.026	2.807	0.420
-1.000	0.900	0.097	0.307	0.031	2.932	0.431
0.250	0.732	0.079	0.232	0.024	3.151	0.470
0.500	0.785	0.085	0.287	0.030	2.731	0.407
0.750	0.861	0.093	0.300	0.030	2.868	0.424
1.000	0.849	0.092	0.315	0.030	2.694	0.386

(0 °)						
Stagger	CL	δCL	CD	δCD	**L/D**	**δ(L/D)**
0.000	0.051	0.006	0.068	0.007	0.745	0.116
-0.250	-0.060	0.007	0.028	0.003	-2.105	0.338
-0.500	0.014	0.002	0.076	0.008	0.187	0.034
-0.750	-0.092	0.010	0.005	0.001	-20.317	6.848
-1.000	0.166	0.018	0.095	0.010	1.746	0.266
0.250	-0.049	0.005	0.004	0.001	-11.577	4.042
0.500	0.082	0.009	0.095	0.010	0.860	0.131
0.750	0.102	0.011	0.056	0.006	1.801	0.277
1.000	-0.003	0.001	0.050	0.006	-0.061	0.028

(12 °)						
Stagger	CL	δCL	CD	δCD	**L/D**	**δ(L/D)**
0.000	1.001	0.108	0.356	0.035	2.813	0.410
-0.250	0.976	0.106	0.419	0.042	2.330	0.343
-0.500	0.949	0.103	0.414	0.042	2.293	0.339
-0.750	0.956	0.103	0.412	0.041	2.321	0.342
-1.000	1.037	0.112	0.423	0.042	2.450	0.358
0.250	1.038	0.112	0.348	0.034	2.980	0.431
0.500	1.086	0.117	0.443	0.043	2.451	0.356
0.750	1.186	0.128	0.413	0.038	2.870	0.406
1.000	1.215	0.131	0.452	0.037	2.685	0.363

(2 °)						
Stagger	CL	δCL	CD	δCD	**L/D**	**δ(L/D)**
0.000	0.193	0.021	0.089	0.010	2.155	0.328
-0.250	0.193	0.021	0.101	0.011	1.903	0.289
-0.500	0.122	0.013	0.088	0.010	1.384	0.211
-0.750	0.100	0.011	0.034	0.004	2.956	0.465
-1.000	0.211	0.023	0.066	0.007	3.197	0.489
0.250	0.320	0.034	0.115	0.012	2.791	0.424
0.500	0.222	0.024	0.114	0.012	1.946	0.296
0.750	0.193	0.021	0.105	0.011	1.834	0.279
1.000	0.206	0.022	0.113	0.012	1.828	0.276

(16 °)						
Stagger	CL	δCL	CD	δCD	**L/D**	**δ(L/D)**
0.000	1.093	0.119	0.540	0.053	2.025	0.297
-0.250	1.044	0.113	0.563	0.056	1.855	0.274
-0.500	1.010	0.110	0.537	0.054	1.882	0.279
-0.750	0.972	0.105	0.513	0.052	1.894	0.281
-1.000	1.038	0.113	0.514	0.051	2.020	0.297
0.250	1.192	0.129	0.559	0.053	2.132	0.308
0.500	1.283	0.140	0.687	0.065	1.867	0.269
0.750	1.376	0.150	0.687	0.062	2.003	0.283
1.000	1.413	0.154	0.710	0.057	1.990	0.268

F.3 Filled Spreadsheets:

Clean Speed at 15 m/s											
With Wing and Stand											
Angle of attack (deg)	Fx (N) (Normal)			Fz (N) (Axial)			Ty (Nmm)			Speed	
	adjusted	measured	TRUE	adjusted	measured	TRUE	adjusted	measured	TRUE	Pressure (Pa)	Speed (m/s)
-4	-1.750	-1.966	-0.216	-0.005	-0.044	-0.040	-38.260	-70.521	-32.260	137.481	15.327
-2	-1.749	-1.749	0.000	-0.039	-0.103	-0.064	-38.402	-41.318	-2.916	140.027	15.469
0	-1.750	-1.529	0.221	-0.077	-0.151	-0.074	-38.499	-12.372	26.127	140.582	15.499
2	-1.750	-1.294	0.456	-0.083	-0.200	-0.117	-38.513	17.204	55.717	135.382	15.210
4	-1.750	-1.006	0.744	-0.133	-0.244	-0.111	-38.414	55.244	93.658	137.017	15.301
8	-1.749	-0.557	1.193	-0.214	-0.247	-0.033	-38.211	112.951	151.162	139.631	15.447
12	-1.750	-0.408	1.342	-0.264	-0.338	-0.074	-37.785	124.597	162.382	138.210	15.368
14	-1.751	-0.396	1.355	-0.298	-0.383	-0.085	-37.347	124.025	161.372	136.633	15.280

Absolute Pressure (hPa) =	1013.000
Ambient Temp (Deg Celcius) =	21.700
ϕ (Relative humidity %) =	25.000

Density of air (kg/m³)	**1.194**
Saturation vapor pressure	25.958
Vapor pressure of water	6.489

Stagger 1.00c

With Wing and Stand

Angle of attack (deg)	Fx (N) (Normal)			Fz (N) (Axial)			Ty (Nmm)			Speed	
	adjusted	measured	TRUE	adjusted	measured	TRUE	adjusted	measured	TRUE	Pressure (Pa)	Speed (m/s)
-4	-2.752	-3.495	-0.742	0.397	0.363	-0.034	-182.237	-337.953	-155.716	138.539	15.386
-2	-2.758	-3.016	-0.258	0.365	0.202	-0.163	-183.310	-245.914	-62.604	144.133	15.694
0	-2.768	-2.796	-0.028	0.284	0.101	-0.184	-185.656	-199.295	-13.639	145.847	15.787
2	-2.778	-2.354	0.424	0.218	-0.079	-0.298	-187.138	-108.155	78.983	145.802	15.784
4	-2.776	-2.004	0.772	0.137	-0.192	-0.329	-188.658	-38.075	150.583	141.873	15.570
8	-2.778	-1.016	1.763	0.030	-0.371	-0.402	-190.196	165.431	355.627	138.353	15.376
12	-2.767	-0.286	2.481	-0.112	-0.362	-0.251	-191.110	313.276	504.386	134.635	15.168
16	-2.746	0.016	2.762	-0.253	-0.548	-0.295	-190.847	349.059	539.906	124.643	14.594

Stand Alone

Angle of attack (deg)	Fx (N) (Normal)			Fz (N) (Axial)			Ty (Nmm)			Speed	
	adjusted	measured	TRUE	adjusted	measured	TRUE	adjusted	measured	TRUE	Pressure (Pa)	Speed (m/s)
-4.000	-1.577	-1.619	-0.041	0.097	0.001	-0.095	-26.383	-30.639	-4.256	141.199	15.533
-2.000	-1.580	-1.612	-0.032	0.065	-0.021	-0.086	-26.932	-30.810	-3.878	140.812	15.512
0.000	-1.584	-1.606	-0.022	0.034	-0.046	-0.079	-27.255	-30.889	-3.634	141.073	15.526
2.000	-1.584	-1.599	-0.014	0.009	-0.072	-0.081	-27.564	-30.965	-3.402	144.142	15.694
4.000	-1.581	-1.589	-0.008	-0.027	-0.106	-0.079	-27.910	-30.794	-2.884	141.123	15.529
8.000	-1.579	-1.571	0.008	-0.093	-0.186	-0.093	-28.323	-30.280	-1.957	140.607	15.501
12.000	-1.576	-1.545	0.032	-0.155	-0.252	-0.097	-28.477	-29.222	-0.745	140.693	15.505
16.000	-1.554	-1.515	0.039	-0.221	-0.314	-0.094	-28.501	-27.808	0.693	141.088	15.527

Stagger 0.75c

With Wing and Stand

Angle of attack (deg)	Fx (N) (Normal)			Fz (N) (Axial)			Ty (Nmm)			Speed	
	adjusted	measured	TRUE	adjusted	measured	TRUE	adjusted	measured	TRUE	Pressure (Pa)	Speed (m/s)
-4	-2.717	-3.348	-0.631	0.358	0.304	-0.054	-172.398	-299.984	-127.586	139.520	15.441
-2	-2.727	-3.001	-0.274	0.313	0.188	-0.125	-174.049	-235.848	-61.799	141.737	15.563
0	-2.737	-2.534	0.203	0.213	0.002	-0.211	-176.927	-144.158	32.769	147.828	15.894
2	-2.740	-2.332	0.408	0.219	-0.077	-0.296	-176.812	-104.852	71.960	146.066	15.799
4	-2.740	-1.665	1.075	0.097	-0.273	-0.370	-178.970	27.406	206.376	142.360	15.597
8	-2.738	-0.942	1.795	0.002	-0.359	-0.362	-180.241	172.304	352.545	139.710	15.451
12	-2.725	-0.306	2.419	-0.122	-0.364	-0.242	-180.921	294.309	475.230	135.662	15.226
16	-2.714	0.019	2.733	-0.212	-0.521	-0.309	-180.884	335.246	516.130	127.266	14.747

Stand Alone

Angle of attack (deg)	Fx (N) (Normal)			Fz (N) (Axial)			Ty (Nmm)			Speed	
	adjusted	measured	TRUE	adjusted	measured	TRUE	adjusted	measured	TRUE	Pressure (Pa)	Speed (m/s)
-4	-1.553	-1.588	-0.036	0.099	0.004	-0.094	-21.662	-25.915	-4.253	137.874	15.349
-2	-1.552	-1.583	-0.031	0.098	0.004	-0.095	-21.724	-26.034	-4.311	137.761	15.343
0	-1.559	-1.571	-0.012	0.062	-0.030	-0.092	-22.223	-26.050	-3.826	137.943	15.353
2	-1.561	-1.564	-0.003	0.026	-0.067	-0.093	-22.678	-26.104	-3.426	140.177	15.477
4	-1.559	-1.557	0.002	-0.024	-0.097	-0.073	-23.190	-26.041	-2.852	139.190	15.422
8	-1.552	-1.547	0.005	-0.087	-0.173	-0.086	-23.630	-25.933	-2.304	141.670	15.559
12	-1.548	-1.528	0.020	-0.115	-0.248	-0.134	-23.731	-25.280	-1.548	143.408	15.654
16	-1.525	-1.502	0.023	-0.213	-0.311	-0.098	-23.843	-24.174	-0.331	138.098	15.362

Stagger 0.5c

With Wing and Stand

Angle of attack (deg)	Fx (N) (Normal)			Fz (N) (Axial)			Ty (Nmm)			Speed	
	adjusted	measured	TRUE	adjusted	measured	TRUE	adjusted	measured	TRUE	Pressure (Pa)	Speed (m/s)
-4	-2.705	-3.42616	-0.721	0.472	0.367148	-0.105	-161.899	-305.452	-143.553	143.539	15.661
-2	-2.721	-3.04065	-0.320	0.376	0.238116	-0.138	-164.743	-238.334	-73.591	145.204	15.752
0	-2.720	-2.55827	0.161	0.319	0.0462986	-0.273	-166.226	-146.469	19.757	144.576	15.718
2	-2.718	-2.25663	0.461	0.223	-0.0758669	-0.299	-168.350	-89.8009	78.549	144.059	15.690
4	-2.717	-1.91658	0.800	0.175	-0.189637	-0.364	-169.442	-26.2045	143.238	140.340	15.486
8	-2.718	-1.10287	1.615	0.036	-0.352506	-0.389	-171.190	129.04	300.230	137.134	15.308
12	-2.710	-0.56503	2.145	-0.069	-0.400492	-0.331	-172.088	231.525	403.613	129.311	14.865
16	-2.691	-0.183451	2.507	-0.217	-0.582172	-0.365	-172.288	284.125	456.413	123.190	14.509

Stand Alone

Angle of attack (deg)	Fx (N) (Normal)			Fz (N) (Axial)			Ty (Nmm)			Speed	
	adjusted	measured	TRUE	adjusted	measured	TRUE	adjusted	measured	TRUE	Pressure (Pa)	Speed (m/s)
-4	-1.604	-1.637	-0.033	0.027	-0.076	-0.103	-20.418	-24.977	-4.560	137.077	15.305
-2	-1.608	-1.623	-0.016	-0.007	-0.086	-0.079	-20.964	-25.094	-4.130	138.613	15.390
0	-1.608	-1.616	-0.008	-0.042	-0.119	-0.077	-21.488	-25.226	-3.738	138.574	15.388
2	-1.604	-1.611	-0.006	-0.081	-0.164	-0.083	-22.005	-25.305	-3.300	138.942	15.408
4	-1.608	-1.607	0.002	-0.109	-0.200	-0.091	-22.170	-25.371	-3.202	141.877	15.570
8	-1.605	-1.597	0.009	-0.164	-0.269	-0.105	-22.659	-25.284	-2.625	142.811	15.622
12	-1.599	-1.581	0.018	-0.242	-0.334	-0.092	-23.052	-24.978	-1.926	142.715	15.616
16	-1.584	-1.557	0.027	-0.330	-0.388	-0.058	-23.224	-24.245	-1.021	140.509	15.495

Stagger 0.25

With Wing and Stand

Angle of attack (deg)	Fx (N) (Normal)			Fz (N) (Axial)			Ty (Nmm)			Speed	
	adjusted	measured	TRUE	adjusted	measured	TRUE	adjusted	measured	TRUE	Pressure (Pa)	Speed (m/s)
-4	-2.680	-3.510	-0.830	0.354	0.350	-0.005	-154.048	-306.432	-152.384	137.730	15.341
-2	-2.692	-2.706	-0.014	0.282	0.077	-0.206	-156.528	-167.014	-10.486	140.427	15.491
0	-2.699	-2.811	-0.112	0.218	0.113	-0.105	-158.251	-187.322	-29.071	146.073	15.799
2	-2.702	-2.051	0.651	0.142	-0.160	-0.301	-159.955	-50.141	109.814	140.650	15.503
4	-2.702	-1.823	0.878	0.102	-0.237	-0.339	-160.699	-9.551	151.148	144.734	15.726
8	-2.698	-1.169	1.529	-0.044	-0.354	-0.311	-162.800	109.719	272.519	139.971	15.465
12	-2.683	-0.571	2.112	-0.190	-0.392	-0.202	-163.718	218.928	382.646	134.584	15.165
16	-2.654	-0.225	2.429	-0.342	-0.631	-0.289	-163.486	259.578	423.064	129.333	14.866

Stand Alone

Angle of attack (deg)	Fx (N) (Normal)			Fz (N) (Axial)			Ty (Nmm)			Speed	
	adjusted	measured	TRUE	adjusted	measured	TRUE	adjusted	measured	TRUE	Pressure (Pa)	Speed (m/s)
-4	-1.583	-1.618	-0.036	0.035	-0.067	-0.102	-17.610	-22.380	-4.770	138.368	15.377
-2	-1.588	-1.601	-0.013	0.002	-0.096	-0.098	-18.195	-22.578	-4.383	139.107	15.418
0	-1.585	-1.594	-0.009	-0.031	-0.127	-0.096	-18.665	-22.606	-3.940	138.964	15.410
2	-1.586	-1.589	-0.003	-0.052	-0.151	-0.100	-18.989	-22.756	-3.767	139.226	15.424
4	-1.588	-1.583	0.005	-0.075	-0.181	-0.106	-19.238	-22.771	-3.534	138.436	15.380
8	-1.578	-1.568	0.011	-0.152	-0.256	-0.104	-20.005	-22.450	-2.446	137.513	15.329
12	-1.575	-1.546	0.029	-0.228	-0.320	-0.092	-20.400	-22.086	-1.686	137.731	15.341
16	-1.570	-1.522	0.048	-0.289	-0.385	-0.096	-20.583	-21.399	-0.816	139.710	15.451

Stagger 0

With Wing and Stand

Angle of attack (deg)	Fx (N) (Normal)			Fz (N) (Axial)			Ty (Nmm)			Speed	
	adjusted	measured	TRUE	adjusted	measured	TRUE	adjusted	measured	TRUE	Pressure (Pa)	Speed (m/s)
-4	-2.653	-3.519	-0.866	0.328	0.335	0.007	-144.223	-297.891	-153.668	135.441	15.213
-2	-2.661	-2.846	-0.185	0.273	0.116	-0.157	-146.051	-188.327	-42.276	138.709	15.396
0	-2.667	-2.579	0.088	0.221	0.015	-0.206	-147.556	-141.564	5.992	140.191	15.478
2	-2.671	-2.279	0.393	0.161	-0.094	-0.255	-149.182	-90.168	59.014	142.470	15.603
4	-2.673	-1.938	0.735	0.087	-0.197	-0.284	-150.652	-32.303	118.349	141.583	15.554
8	-2.672	-0.959	1.713	-0.038	-0.368	-0.330	-152.665	138.268	290.933	138.837	15.403
12	-2.659	-0.611	2.048	-0.172	-0.400	-0.228	-153.894	197.989	351.883	135.611	15.223
16	-2.641	-0.388	2.253	-0.283	-0.624	-0.341	-154.202	218.518	372.720	130.570	14.937

Stand Alone

Angle of attack (deg)	Fx (N) (Normal)			Fz (N) (Axial)			Ty (Nmm)			Speed	
	adjusted	measured	TRUE	adjusted	measured	TRUE	adjusted	measured	TRUE	Pressure (Pa)	Speed (m/s)
-4	-1.532	-1.569	-0.037	0.022	-0.071	-0.092	-15.316	-20.026	-4.710	138.309	15.373
-2	-1.544	-1.556	-0.012	-0.025	-0.100	-0.075	-15.999	-20.327	-4.328	142.737	15.618
0	-1.535	-1.548	-0.013	-0.052	-0.122	-0.070	-16.467	-20.349	-3.882	139.941	15.464
2	-1.534	-1.541	-0.006	-0.080	-0.170	-0.089	-16.829	-20.490	-3.661	141.894	15.571
4	-1.535	-1.534	0.002	-0.113	-0.197	-0.084	-17.245	-20.376	-3.131	137.893	15.350
8	-1.531	-1.523	0.008	-0.183	-0.254	-0.070	-17.879	-20.429	-2.550	138.667	15.393
12	-1.519	-1.507	0.012	-0.246	-0.320	-0.075	-18.282	-20.304	-2.021	136.779	15.288
16	-1.514	-1.487	0.027	-0.294	-0.379	-0.085	-18.389	-19.963	-1.575	137.360	15.321

Stagger -0.25

With Wing and Stand

Angle of attack (deg)	Fx (N) (Normal)			Fz (N) (Axial)			Ty (Nmm)			Speed	
	adjusted	measured	TRUE	adjusted	measured	TRUE	adjusted	measured	TRUE	Pressure (Pa)	Speed (m/s)
-4	-2.545	-3.531	-0.986	0.309	0.322	0.013	-151.244	-329.382	-178.138	132.903	15.070
-2	-2.554	-3.053	-0.499	0.252	0.170	-0.082	-153.264	-250.936	-97.672	139.162	15.421
0	-2.563	-2.698	-0.134	0.183	0.037	-0.146	-155.393	-187.347	-31.954	141.491	15.549
2	-2.569	-2.164	0.404	0.122	-0.160	-0.282	-156.997	-93.360	63.637	144.490	15.713
4	-2.573	-1.815	0.758	0.063	-0.274	-0.337	-158.334	-32.026	126.308	139.545	15.442
8	-2.576	-1.022	1.554	-0.036	-0.435	-0.399	-159.991	111.820	271.811	138.308	15.373
12	-2.568	-0.594	1.975	-0.175	-0.534	-0.359	-161.439	183.773	345.212	132.018	15.020
16	-2.546	-0.339	2.207	-0.321	-0.749	-0.428	-161.786	214.006	375.792	132.011	15.019

Stand Alone

Angle of attack (deg)	Fx (N) (Normal)			Fz (N) (Axial)			Ty (Nmm)			Speed	
	adjusted	measured	TRUE	adjusted	measured	TRUE	adjusted	measured	TRUE	Pressure (Pa)	Speed (m/s)
-4	-1.552	-1.597	-0.045	0.056	-0.040	-0.095	-17.842	-22.724	-4.882	138.886	15.405
-2	-1.558	-1.583	-0.026	0.035	-0.055	-0.090	-18.159	-22.945	-4.786	141.097	15.528
0	-1.565	-1.578	-0.013	0.011	-0.078	-0.089	-18.666	-23.085	-4.419	142.022	15.578
2	-1.574	-1.576	-0.002	-0.012	-0.100	-0.089	-19.067	-23.228	-4.161	142.177	15.587
4	-1.569	-1.570	-0.001	-0.058	-0.148	-0.090	-19.622	-23.320	-3.698	140.155	15.476
8	-1.565	-1.561	0.004	-0.126	-0.216	-0.090	-20.404	-23.475	-3.071	140.850	15.514
12	-1.559	-1.550	0.009	-0.202	-0.278	-0.077	-20.946	-23.563	-2.616	142.239	15.590
16	-1.559	-1.533	0.027	-0.254	-0.337	-0.083	-21.172	-23.246	-2.074	142.745	15.618

Stagger -0.5

With Wing and Stand

Angle of attack (deg)	Fx (N) (Normal)			Fz (N) (Axial)			Ty (Nmm)			Speed	
	adjusted	measured	TRUE	adjusted	measured	TRUE	adjusted	measured	TRUE	Pressure (Pa)	Speed (m/s)
-4	-2.548	-3.408	-0.861	0.315	0.303	-0.012	-160.493	-324.747	-164.254	133.223	15.088
-2	-2.555	-3.175	-0.620	0.267	0.228	-0.039	-162.139	-284.871	-122.732	135.920	15.240
0	-2.563	-2.547	0.016	0.227	0.000	-0.227	-163.434	-169.248	-5.814	139.084	15.416
2	-2.567	-2.315	0.252	0.166	-0.091	-0.257	-165.131	-126.493	38.638	143.266	15.646
4	-2.573	-1.924	0.648	0.061	-0.227	-0.288	-167.402	-54.068	113.334	141.145	15.530
8	-2.573	-1.027	1.545	-0.023	-0.423	-0.399	-168.885	115.471	284.356	139.548	15.442
12	-2.563	-0.625	1.938	-0.164	-0.538	-0.374	-170.227	181.741	351.968	132.476	15.046
16	-2.544	-0.459	2.085	-0.302	-0.705	-0.403	-170.436	200.529	370.965	129.086	14.852

Stand Alone

Angle of attack (deg)	Fx (N) (Normal)			Fz (N) (Axial)			Ty (Nmm)			Speed	
	adjusted	measured	TRUE	adjusted	measured	TRUE	adjusted	measured	TRUE	Pressure (Pa)	Speed (m/s)
-4	-1.579	-1.618	-0.039	0.061	-0.037	-0.098	-20.306	-24.873	-4.568	135.702	15.228
-2	-1.583	-1.608	-0.024	0.034	-0.056	-0.090	-20.939	-25.048	-4.109	134.859	15.180
0	-1.590	-1.602	-0.012	0.001	-0.076	-0.077	-21.444	-25.151	-3.707	134.029	15.134
2	-1.593	-1.598	-0.005	-0.030	-0.116	-0.086	-21.899	-25.428	-3.529	135.247	15.202
4	-1.598	-1.592	0.005	-0.062	-0.152	-0.090	-22.347	-25.454	-3.107	133.681	15.114
8	-1.594	-1.583	0.011	-0.126	-0.222	-0.097	-23.055	-25.724	-2.669	134.615	15.167
12	-1.588	-1.571	0.017	-0.194	-0.274	-0.080	-23.511	-25.754	-2.242	135.476	15.215
16	-1.575	-1.550	0.025	-0.254	-0.337	-0.082	-23.820	-25.388	-1.569	134.846	15.180

Stagger -0.75

With Wing and Stand

Angle of attack (deg)	Fx (N) (Normal)			Fz (N) (Axial)			Ty (Nmm)			Speed	
	adjusted	measured	TRUE	adjusted	measured	TRUE	adjusted	measured	TRUE	Pressure (Pa)	Speed (m/s)
-4	-2.536	-3.475	-0.940	0.311	0.307	-0.004	-169.133	-352.758	-183.625	136.039	15.247
-2	-2.543	-3.022	-0.479	0.264	0.186	-0.078	-170.805	-269.990	-99.185	140.905	15.517
0	-2.552	-2.753	-0.201	0.184	0.086	-0.098	-173.210	-219.172	-45.962	143.135	15.639
2	-2.557	-2.365	0.192	0.109	-0.058	-0.167	-175.075	-141.746	33.329	140.251	15.481
4	-2.559	-1.862	0.696	0.041	-0.236	-0.277	-176.412	-42.973	133.439	141.006	15.523
8	-2.557	-1.144	1.412	-0.072	-0.407	-0.335	-178.056	98.466	276.522	136.371	15.265
12	-2.548	-0.608	1.941	-0.192	-0.552	-0.359	-179.029	192.580	371.609	131.958	15.016
16	-2.531	-0.508	2.022	-0.291	-0.673	-0.382	-179.133	201.092	380.225	129.853	14.896

Stand Alone

Angle of attack (deg)	Fx (N) (Normal)			Fz (N) (Axial)			Ty (Nmm)			Speed	
	adjusted	measured	TRUE	adjusted	measured	TRUE	adjusted	measured	TRUE	Pressure (Pa)	Speed (m/s)
-4	-1.595	-1.638	-0.043	0.058	-0.045	-0.103	-21.434	-26.646	-5.213	140.589	15.500
-2	-1.600	-1.628	-0.028	0.019	-0.062	-0.082	-22.198	-26.924	-4.727	143.538	15.661
0	-1.605	-1.617	-0.012	-0.019	-0.108	-0.089	-22.829	-27.189	-4.361	144.445	15.711
2	-1.605	-1.616	-0.011	-0.030	-0.137	-0.107	-22.898	-27.148	-4.249	140.873	15.515
4	-1.605	-1.612	-0.007	-0.070	-0.166	-0.096	-23.544	-27.235	-3.692	142.758	15.619
8	-1.604	-1.598	0.005	-0.148	-0.236	-0.089	-24.471	-27.474	-3.003	141.585	15.554
12	-1.596	-1.581	0.015	-0.217	-0.293	-0.076	-25.012	-27.250	-2.238	141.818	15.567
16	-1.588	-1.560	0.028	-0.280	-0.350	-0.070	-25.340	-26.704	-1.364	144.433	15.710

Stagger -1

With Wing and Stand

Angle of attack (deg)	Fx (N) (Normal)			Fz (N) (Axial)			Ty (Nmm)			Speed	
	adjusted	measured	TRUE	adjusted	measured	TRUE	adjusted	measured	TRUE	Pressure (Pa)	Speed (m/s)
-4	-2.572	-3.067	-0.496	0.294	0.187	-0.106	-180.448	-290.458	-110.010	134.252	15.146
-2	-2.581	-2.863	-0.283	0.225	0.114	-0.111	-182.619	-249.854	-67.235	134.515	15.161
0	-2.583	-2.255	0.328	0.188	-0.113	-0.301	-183.764	-126.381	57.383	138.964	15.410
2	-2.589	-2.174	0.415	0.092	-0.140	-0.232	-186.031	-110.072	75.959	135.707	15.228
4	-2.590	-1.524	1.066	0.041	-0.345	-0.386	-186.956	20.890	207.846	137.271	15.316
8	-2.580	-0.801	1.779	-0.106	-0.433	-0.327	-188.954	172.534	361.488	132.000	15.019
12	-2.570	-0.532	2.038	-0.213	-0.531	-0.318	-189.621	214.686	404.307	128.284	14.806
16	-2.536	-0.428	2.108	-0.411	-0.738	-0.326	-189.285	215.931	405.216	128.094	14.795

Stand Alone

Angle of attack (deg)	Fx (N) (Normal)			Fz (N) (Axial)			Ty (Nmm)			Speed	
	adjusted	measured	TRUE	adjusted	measured	TRUE	adjusted	measured	TRUE	Pressure (Pa)	Speed (m/s)
-4	-1.632	-1.660	-0.028	0.059	-0.042	-0.101	-26.025	-30.769	-4.744	136.982	15.299
-2	-1.636	-1.650	-0.015	0.034	-0.079	-0.113	-26.578	-31.212	-4.634	137.782	15.344
0	-1.638	-1.642	-0.004	0.008	-0.105	-0.113	-27.100	-31.394	-4.295	136.295	15.261
2	-1.638	-1.637	0.000	-0.022	-0.144	-0.121	-27.667	-31.511	-3.844	137.486	15.328
4	-1.639	-1.632	0.008	-0.064	-0.172	-0.108	-28.280	-31.524	-3.244	137.089	15.305
8	-1.634	-1.622	0.013	-0.160	-0.234	-0.074	-29.452	-31.705	-2.252	135.907	15.239
12	-1.625	-1.603	0.021	-0.221	-0.299	-0.079	-29.912	-31.542	-1.630	135.366	15.209
16	-1.611	-1.581	0.030	-0.296	-0.368	-0.072	-30.279	-30.798	-0.520	137.296	15.317

F.4 Sample Spreadsheets (Method used in Tabulating and Calculating)

In this section, the lift, drag, coefficients, instrument error attached and wall corrections were applied and were tabulated as shown below. Similar spreadsheets were created for all nine configurations.

Wall Effect Corrections and CL, CD, and CM																	
Corrected Angle of attack (deg)	Corrected Angle of Attack (rad)	Angle of Attack (rad)	Angle of attack (deg)	F(x) Normal	F(z) Axial	Ty (Nmm)	Lift(N)	Corrected Lift(N)	Drag (N)	Corrected Drag (N)	Moment (Nm)	CL (inc)	Corrected CL (inc)	CD (inc)	Corrected CD (inc)	CD wall effect Corrected	CM (Inc)
-4.72	-0.082	-0.070	-4	-0.829	0.099	-148.959	-0.820	-0.818	0.156	0.167	-0.149	-0.423	-0.422	0.081	0.086	0.087	-1.317
-2.15	-0.037	-0.035	-2	-0.173	0.081	-37.948	-0.170	-0.170	0.087	0.088	-0.038	-0.086	-0.086	0.044	0.044	0.044	-0.328
0.09	0.002	0.000	0	0.102	0.136	9.874	0.102	0.101	0.136	0.136	0.010	0.051	0.051	0.068	0.068	0.068	0.084
2.33	0.041	0.035	2	0.399	0.166	62.675	0.393	0.392	0.180	0.182	0.063	0.193	0.193	0.088	0.089	0.089	0.527
4.60	0.080	0.070	4	0.733	0.200	121.480	0.718	0.715	0.250	0.258	0.121	0.355	0.353	0.124	0.127	0.128	1.028
9.42	0.164	0.140	8	1.705	0.260	293.483	1.653	1.640	0.495	0.535	0.293	0.832	0.826	0.249	0.270	0.284	2.532
13.72	0.239	0.209	12	2.036	0.153	353.904	1.960	1.942	0.573	0.632	0.354	1.011	1.001	0.296	0.326	0.356	3.125
17.88	0.312	0.279	16	2.227	0.256	374.295	2.070	2.040	0.860	0.928	0.374	1.109	1.093	0.461	0.497	0.540	3.433

		Error Analysis																				
		Angle (Degree)	Angle (Radians)	Pressure (Pa)	Velocity (m/s)	Normal Force (N)	Axial Force (N)	Lift (N)	Drag (N)	Moment (N.m)	qinf	δq	δV	δL	δD	Angle of Attack (Deg)	Angle (Radians)	CL	δCL	CD	δCD	CM	δCM
A = c*s	1.4E-02	-4.720	-0.068	135.441	15.213	-0.829	0.099	-0.820	0.167	-0.149	137.706	0.5647	0.0312	0.0028	0.0029	-4.7197	-0.0676	-0.422	0.045	0.087	0.009	-1.317	0.141
SA = c*c*s	8.2E-04	-2.146	0.009	138.709	15.396	-0.173	0.081	-0.170	0.088	-0.038	141.029	0.5647	0.0308	0.0028	0.0028	-2.1456	0.0086	-0.086	0.009	0.044	0.005	-0.328	0.035
δA	0.0015	0.086	0.086	140.191	15.478	0.102	0.136	0.102	0.136	0.010	142.536	0.5647	0.0307	0.0028	0.0028	0.0861	0.0856	0.051	0.006	0.068	0.007	0.084	0.009
δSC	0.0001	2.328	0.162	142.470	15.603	0.399	0.166	0.393	0.182	0.063	144.853	0.5647	0.0304	0.0028	0.0028	2.3282	0.1624	0.193	0.021	0.089	0.010	0.527	0.056
		4.603	0.237	141.583	15.554	0.733	0.200	0.718	0.258	0.121	143.951	0.5647	0.0305	0.0028	0.0028	4.6027	0.2375	0.353	0.038	0.128	0.014	1.028	0.110
		9.415	0.304	138.837	15.403	1.705	0.260	1.653	0.535	0.293	141.159	0.5647	0.0308	0.0028	0.0031	9.4152	0.3039	0.826	0.089	0.284	0.029	2.532	0.271
		13.718	0.370	135.611	15.223	2.036	0.153	1.960	0.632	0.354	137.879	0.5647	0.0312	0.0029	0.0032	13.7183	0.3701	1.001	0.108	0.356	0.035	3.125	0.334
		17.885	0.441	130.570	14.937	2.227	0.256	2.070	0.928	0.374	132.754	0.5647	0.0318	0.0029	0.0033	17.8847	0.4414	1.093	0.119	0.540	0.053	3.433	0.367

Stagger 0								
Angle of Attack (Deg)	CL	δCL	CD	δCD	CM	δCM	L/D	δ(L/D)
-4.720	-0.422	0.045	0.087	0.009	-1.317	0.141	-4.852	0.7352071
-2.146	-0.086	0.009	0.044	0.005	-0.328	0.035	-1.932	0.3003357
0.086	0.051	0.006	0.068	0.007	0.084	0.009	0.745	0.1156284
2.328	0.193	0.021	0.089	0.010	0.527	0.056	2.155	0.3281713
4.603	0.353	0.038	0.128	0.014	1.028	0.110	2.764	0.4189898
9.415	0.826	0.089	0.284	0.029	2.532	0.271	2.913	0.4316567
13.718	1.001	0.108	0.356	0.035	3.125	0.334	2.813	0.4098943
17.885	1.093	0.119	0.540	0.053	3.433	0.367	2.025	0.2966503